

# Regge analysis of the $\pi\pi$ scattering amplitude

I. Caprini<sup>1</sup>, G. Colangelo<sup>2</sup> and H. Leutwyler<sup>2</sup>

<sup>1</sup> Horia Hulubei National Institute for Physics and Nuclear Engineering, P.O.B. MG-6, 077125 Magurele, Romania

<sup>2</sup> Albert Einstein Center for Fundamental Physics, Institute for Theoretical Physics, University of Bern, Sidlerstrasse 5, CH-3012 Bern, Switzerland

December 21, 2011

**Abstract.** The theoretical predictions for the subtraction constants lead to a very accurate dispersive representation of the  $\pi\pi$  scattering amplitude below 0.8 GeV. The extension of this representation up to the maximum energy of validity of the Roy equations (1.15 GeV) requires a more precise input at high energies. In this paper we determine the trajectories and residues of the leading Regge contributions to the  $\pi\pi$  amplitude (Pomeron,  $f$  and  $\rho$ ), using factorization, phenomenological parametrizations of the  $\pi N$  and  $NN$  total cross sections at high energy and a set of sum rules which connect the high and low energy properties of  $\pi\pi$  scattering. We find that nonleading Regge terms are necessary in order to achieve a smooth transition from the partial waves to the Regge representation at or below 2 GeV. We obtain thus a Regge representation consistent both with the experimental information at high energies and the Roy equations for the partial waves with  $\ell \leq 4$ . The uncertainties in our result for the Regge parameters are sizable but in the solutions of the Roy equations, these only manifest themselves above  $K\bar{K}$  threshold.

## 1 Motivation

Low energy pion physics has become a precision laboratory: the chiral symmetry properties of the Standard Model can now be compared with low energy precision experiments, using Chiral Perturbation Theory ( $\chi$ PT), dispersion theory and numerical simulations of QCD on a lattice. In principle, as illustrated by the prediction for the magnetic moment of the muon, physics beyond the Standard Model can show up at low energies, provided the quantity of interest can not only be measured accurately, but can also be calculated to sufficient precision. In this context, the interaction among the pions and in particular, the elastic  $\pi\pi$  scattering amplitude play a crucial role.

The Roy equations [1] provide a suitable framework for the low energy analysis of the  $\pi\pi$  scattering amplitude, as they fully incorporate the basic properties that follow from analyticity, unitarity and crossing symmetry. They express the real parts of the partial waves as integrals over the imaginary parts that extend over all energies. The high energy behaviour of the imaginary parts thus enters the analysis, even if the Roy equations are evaluated only at low energy. More specifically, the contributions from the high energy region are contained in the so-called *driving terms*. Near the  $\pi\pi$  threshold, these terms are very small. Accordingly, the results for the threshold parameters are not sensitive to the high energy contributions. The driving terms, however, grow with the energy. In [2, 4], where the threshold parameters and the coupling constants of the effective chiral  $SU(2) \times SU(2)$  Lagrangian

relevant for  $\pi\pi$  scattering are determined to high accuracy, the Roy equations are solved only below 0.8 GeV. On general grounds [1] these equations are valid in the region<sup>1</sup>  $s \leq 68 M_\pi^2$ , i.e. for  $\sqrt{s} \leq 1.15$  GeV, but in order to use them we need an accurate evaluation of the driving terms. This calls for a better understanding of the imaginary parts at high energies and motivates the present work.

For  $\pi\pi$  scattering, several sets of data at high energies are available from indirect experiments [7–13]. These were analyzed in the late seventies, both in the frame of the Lovelace-Shapiro-Veneziano (LSV) model [14] and by means of various dispersive sum rules [15–22]. While the determination of the structure in the resonance region gradually made progress [23–31], the Regge analysis of the  $\pi\pi$  scattering amplitude was for a long time practically abandoned.

The Regge parametrization used in [2–4] is based on Pennington's analysis [21]. This input was subject to a criticism in [32], where an alternative Regge parametrization was proposed. As shown in [33], the driving terms and the  $S$  and  $P$ -phase shifts below 0.8 GeV are practically insensitive to the difference between the Regge parametrization used in [2] and that proposed in [32]. However, for extending the Roy analysis up to 1.15 GeV, an update of the Regge parametrization used as input is necessary. Ir-

<sup>1</sup> The maximum energy can be increased by using, instead of fixed- $t$  dispersion relations as in the standard approach, more general dispersion relations along curves in the Mandelstam plane [5, 6].

respective of the very modest impact it has on the region below 0.8 GeV, credit is due to Peláez and Ynduráin [32] for pointing out the need of improving the Regge representation used in [2]. In the meantime, these authors and their collaborators gradually improved their own Regge parametrization [34–37]. In the following we will compare our results with the most recent version of this series, [37], more precisely with the variant referred to as “CFD”, which appears to represent the net result of their work.

After a brief introduction to the Regge representation in the next section, we review the phenomenology of the leading Regge trajectories and of the total  $NN$  and  $\pi N$  cross sections and discuss the consequences of factorization for the total  $\pi\pi$  cross sections. The Regge representation used in the present work is specified in section 4. Section 5 contains a short description of the partial wave representation used in the present analysis, and section 6 presents the resulting picture for the total cross sections. In section 7, we introduce the quantitative formulation of duality used in the present work and section 8 discusses the sum rules we are relying on to calculate the  $t$ -dependence of the Regge residues. Details concerning the way in which our analysis is carried out are explained in section 9. Our results for the Regge residues at  $t = 0$  are presented in section 10, while those concerning their  $t$ -dependence are discussed in section 11. A few consistency checks are described in section 12. Finally, in section 13, we present a summary and draw some conclusions.

The paper has four appendices: in appendix A we give a short review of the Regge parametrizations of the  $\pi\pi$  amplitude proposed in the literature. In appendix B we specify the input used when solving the Roy equations for the partial waves (a detailed presentation will be given in a forthcoming paper [38]). In appendix C we provide the explicit expressions of the sum rules used in this analysis and in appendix D we specify some details of the minimization procedure used to impose our constraints. Preliminary results of this work were reported in [39–43].

## 2 Regge poles

The high energy behaviour of soft hadronic and photon-induced reactions can be described in terms of Regge poles and cuts in the angular-momentum plane. A Regge pole actually corresponds to the exchange of an infinite series of particles or resonances with quantum numbers such that they can be produced in the  $t$ -channel. For a detailed account of this framework and its application to meson-nucleon and nucleon-nucleon scattering we refer to the older literature [44–54]. More recent studies [55–75] consider the description of the Pomeron in QCD [56] and applications of Regge theory to diffractive phenomena and deep inelastic  $ep$  scattering at low  $x$  (see the excellent review [61]). For soft hadronic processes, global fits of the  $\pi N$ ,  $KN$  and  $NN$  high energy data sets based on the Regge representation were performed in a systematic way [62], as quoted in the Review of Particle Physics [63, 64]. More sophisticated representations are obtained by including Regge cuts to describe absorption [65, 66], or

by the eikonalization of Regge exchanges in the impact-parameter representations [67–70]. These models extend the validity of the framework to larger momentum transfers and to higher energies, respectively.

The contribution of a Regge pole to a scattering amplitude at large c.m. energy squared  $s$  and small momentum transfer  $t \leq 0$  has the form

$$T(s, t) = -\beta(t) \frac{\exp[-i\pi\alpha(t)] + \tau \left(\frac{s}{s_1}\right)^{\alpha(t)}}{\sin[\pi\alpha(t)]}, \quad (1)$$

where  $\alpha(t)$  and  $\beta(t)$  denote the trajectory and the residue, respectively, and  $\tau$  is the signature, taking the value 1 (−1) for  $C$ -even (odd) trajectories. The scale factor  $s_1$  is usually set equal to 1 GeV<sup>2</sup> and we will adopt this convention. Like the scattering amplitude  $T(s, t)$  itself, the residue  $\beta(t)$  of a Regge pole is a dimensionless quantity.

The trajectories  $\alpha(t)$  and the residues  $\beta(t)$  are analytic functions of  $t$ , with branch points at the unitarity thresholds in the  $t$ -channel. The trajectories are universal, *i.e.* a definite Regge pole in the angular momentum plane is located at the same place  $J = \alpha(t)$  in all processes where it contributes. Information on the trajectories is inferred from the plot of the spin of known resonances versus the square of their mass (Chew-Frautschi diagrams). Throughout this paper, we assume that in the  $t$  region of interest the trajectories are approximately linear<sup>2</sup>

$$\alpha(t) = \alpha(0) + \alpha'(0)t. \quad (2)$$

The residues  $\beta(t)$  are much less known. The zeros of the denominator in (1) give rise to poles of the amplitude – unless the numerator or the residue  $\beta(t)$  vanish there. For positive  $t$ , the poles correspond to the physical resonances situated on the Chew-Frautschi plots. Poles in the spacelike region are unphysical, hence the residue  $\beta(t)$  must vanish if  $\alpha(t) + \frac{1}{2}(1 + \tau)$  is an odd integer and  $t < 0$ . In the literature, this condition is sometimes implemented with factors depending explicitly on  $\alpha(t)$  (see appendix A).

A remarkable property of the residues, which follows from unitarity, is their factorization as a product of two vertices. For the exchange of a Reggeon  $R$  in the process  $a + b \rightarrow c + d$ , factorization reads

$$\beta_R(t) = \gamma_{Rac}(t)\gamma_{Rbd}(t). \quad (3)$$

For particles with spin, this relation holds separately for amplitudes of definite helicity.

In the representation quoted by the Particle Data Group [63], the dominant contribution, the Pomeron, is described as a triple pole in the angular momentum plane, which leads to an increase with energy as the square of a logarithm. Also, at nonleading order, daughter poles as well as Regge cuts arising from the simultaneous exchange of two or more poles contribute [49, 53]. In fact, in exotic channels, where resonances do not occur, the dominating contributions stem from such cuts.

<sup>2</sup> Deviations from linearity were also investigated, see for instance [59].

The position  $\alpha_{cut}(t)$  of the first branch-point arising from the exchange of two Regge poles is determined by the corresponding trajectories. For the exchange of two identical poles, characterized by the linear trajectory  $\alpha(0) + \alpha'(0)t$ , the expression reads [49, 53]

$$\alpha_{cut}(t) = 2\alpha(0) - 1 + \frac{1}{2}\alpha'(0)t. \quad (4)$$

At large  $s$ , a Regge cut contributes as  $s^{\alpha_{cut}(t)}$ , with additional logarithmic factors like  $\ln^\gamma(s/s_c)$ , where the scale  $s_c$  and the exponent  $\gamma$  of the correction are in general unknown [61]. Factorization does not hold for cuts and generally fails for absorption corrections [52], especially at large negative  $t$ .

### 3 Phenomenology of leading trajectories and total cross sections

#### 3.1 $\pi N$ and $NN$ total cross sections

During the last decade, a comprehensive compilation of the hadronic total cross sections was developed by the Compete Collaboration [62]. The Regge fit of the data above 5 GeV, quoted in PDG 2011 [63], is based on the expressions:

$$\begin{aligned} \sigma_{ab}(s) &= B \ln^2(s/s_0) + Z_{ab} + \\ &\quad Y_{1ab}(s_1/s)^{\eta_1} - Y_{2ab}(s_1/s)^{\eta_2}, \\ \sigma_{\bar{a}b}(s) &= B \ln^2(s/s_0) + Z_{ab} + \\ &\quad Y_{1ab}(s_1/s)^{\eta_1} + Y_{2ab}(s_1/s)^{\eta_2}, \end{aligned} \quad (5)$$

where the target particle  $b$  is either a proton ( $p$ ) or a neutron ( $n$ ), and the projectiles  $a$  ( $\bar{a}$ ) are  $p$  or  $\pi^+$ , or their antiparticles.

The first two terms on the right hand side of (5) represent the contribution of the Pomeron. The coefficient  $B$  and the scale  $s_0$  of the logarithmic term are assumed to be universal:

$$B = 0.308 \pm 0.010 \text{ mb}, \quad \sqrt{s_0} = 5.38 \pm 0.50 \text{ GeV}. \quad (6)$$

The universality hypothesis was tested independently in [73, 74].

The coefficients accounting for the energy independent part of the Pomeron contribution to the cross section are

$$Z_{NN} = 35.63 \pm 0.25 \text{ mb}, \quad Z_{\pi^+p} = 20.86 \pm 0.03 \text{ mb}, \quad (7)$$

where the first value is the mean of  $Z_{pp}$  and  $Z_{pn}$  (which agree within errors, indicating that the isospin breaking effects are very small). The numbers (6)–(7) show that – unless the energy is taken so high that  $\ln(s/s_0)$  becomes large compared to 1 – the Pomeron term is approximately independent of the energy.

The remaining terms in (5) account for the leading Regge poles, which for  $NN$  scattering are known to be  $f$ ,  $a_2$ ,  $\rho$  and  $\omega$  [53]. The connection with (1) is provided

by the optical theorem, which relates the total cross sections to the imaginary parts of the corresponding forward amplitudes. At high energies, it yields

$$\sigma_{\text{pole}}(s) \approx \frac{\beta(0)}{s_1} \left( \frac{s}{s_1} \right)^{\alpha(0)-1}. \quad (8)$$

For  $NN$  scattering, the term proportional to  $Y_1$  in (5) collects the contributions of the dominant  $C$ -even trajectories,  $f$  and  $a_2$ , with the intercepts taken to be the same,  $\alpha_f(0) = \alpha_{a_2}(0) = 1 - \eta_1$ , the contributions from lower trajectories being neglected. Likewise, the leading  $C$ -odd trajectories,  $\rho$  and  $\omega$ , are represented by the term proportional to  $Y_2$ , with  $\alpha_\rho(0) = \alpha_\omega(0) = 1 - \eta_2$ . For completeness we quote the values from [63]:

$$\begin{aligned} Y_{1pp} &= 42.53 \pm 0.23 \text{ mb}, & Y_{2pp} &= 33.34 \pm 0.33 \text{ mb} \\ Y_{1pn} &= 40.15 \pm 1.59 \text{ mb}, & Y_{2pn} &= 30.00 \pm 0.96 \text{ mb}. \end{aligned} \quad (9)$$

Using (5) for the collisions of protons or antiprotons on protons and neutrons, we can separate the contributions from the individual trajectories,  $f$ ,  $a_2$ ,  $\rho$  and  $\omega$ :  $Y_{1pp} = Y_{fNN} + Y_{a_2NN}$  and  $Y_{2pp} = Y_{\rho NN} + Y_{\omega NN}$ . If the proton target is replaced by a neutron, the isospin odd contributions from  $\rho$  and  $a_2$  change sign. Hence, the combinations relevant for the scattering on neutrons are given by  $Y_{1pn} = Y_{fNN} - Y_{a_2NN}$  and  $Y_{2pn} = -Y_{\rho NN} + Y_{\omega NN}$ .

At high energies, the cross sections barely show any difference between proton and neutron targets, indicating that  $Y_{a_2NN}$  and  $Y_{\rho NN}$  are small. In early works [46], the  $\rho$  and  $a_2$  contributions to  $pp$  and  $\bar{p}p$  scattering were found to be negligible and in some analyses they were simply dropped [47]. The recent Regge analysis of nucleon-nucleon scattering above 3 GeV reported in [75] confirms that  $f$  and  $\omega$  dominate over  $a_2$  and  $\rho$ , respectively. Indeed, the values obtained from (9),

$$\begin{aligned} Y_{fNN} &= 41.3 \pm 0.8 \text{ mb}, & Y_{a_2NN} &= 1.2 \pm 0.8 \text{ mb}, \\ Y_{\rho NN} &= 1.7 \pm 0.5 \text{ mb}, & Y_{\omega NN} &= 31.7 \pm 0.5 \text{ mb} \end{aligned} \quad (10)$$

show that the couplings of  $a_2$  and  $\rho$  to the nucleons are too small to clearly stick out.

If isospin breaking effects are neglected, only the  $f$  and  $\rho$  trajectories are present in  $\pi N$  scattering, in accord with the fact that two pions in a configuration with even (odd) isospin must carry even (odd) angular momentum, so cannot couple to  $a_2$  or  $\omega$ . The parameters  $Y$  given in [63] for this process are:

$$Y_{f\pi N} = 19.24 \pm 0.18 \text{ mb}, \quad Y_{\rho\pi N} = 6.03 \pm 0.09 \text{ mb}. \quad (11)$$

#### 3.2 Leading trajectories

The intercepts of the leading trajectories can be read off from the powers of  $s$  occurring in the representation (5) for the total cross sections. As mentioned above, this representation describes the Pomeron as a triple pole with

$$\alpha_P(0) = 1. \quad (12)$$

Using the values  $\eta_1 = 0.458 \pm 0.017$  and  $\eta_2 = 0.545 \pm 0.007$  from [63] and enlarging the errors to take into account other results in the literature (see appendix A) we take:

$$\alpha_f(0) = 0.54 \pm 0.05, \quad \alpha_\rho(0) = 0.45 \pm 0.02. \quad (13)$$

As stated above, we assume that in the  $t$  region of interest, the trajectories are adequately approximated by the linear formula (2). For the slope of the Pomeron trajectory, we use the value

$$\alpha'_P(0) = 0.25 \pm 0.05 \text{ GeV}^{-2}, \quad (14)$$

which is consistent with the information on the shape of diffraction peak at high energies (see appendix A).

For  $\alpha_f(t)$  and  $\alpha_\rho(t)$ , we fix the slopes with the requirement that the trajectories pass through the masses squared:  $\alpha_f(M_{f_2}^2) = 2$  and  $\alpha_\rho(M_\rho^2) = 1$ , respectively. Using the experimental values for the masses and adding errors to cover other results quoted in appendix A, we take

$$\begin{aligned} \alpha'_f(0) &= 0.90 \pm 0.05 \text{ GeV}^{-2}, \\ \alpha'_\rho(0) &= 0.91 \pm 0.02 \text{ GeV}^{-2}. \end{aligned} \quad (15)$$

### 3.3 Factorization

We rely on the values derived in section 3.1 in order to extract the Regge parameters of the  $\pi\pi$  amplitude through factorization, using equations (3) and (8). As remarked in section 2, if the particles carry spin, factorization applies to amplitudes of definite helicity. In the forward direction, only the non-flip coupling survives, and factorization holds for each Regge pole contributing to the  $\pi\pi$ ,  $\pi N$  and  $NN$  cross sections [53].

In the case of  $\pi\pi$  scattering the representation (5) reads

$$\begin{aligned} \sigma_{\pi^\pm\pi^\pm}(s) &= B \ln^2(s/s_0) + Z_{\pi\pi} + \\ &Y_{f\pi\pi} (s_1/s)^{\eta_1} \mp Y_{\rho\pi\pi} (s_1/s)^{\eta_2}. \end{aligned} \quad (16)$$

The expression involves the leading Regge terms  $P$ ,  $f$  and  $\rho$ . For the Pomeron, factorization gives the universality of the parameters  $B$  and  $s_0$  and

$$Z_{\pi\pi} = \frac{Z_{\pi N}^2}{Z_{NN}} = 12.2 \pm 0.1 \text{ mb}. \quad (17)$$

This is to be compared with the number obtained from  $Z_{\pi N}$  with the quark counting rule:  $Z_{\pi\pi} \approx \frac{2}{3} Z_{\pi N} \approx 14 \text{ mb}$ . For the  $Y$  parameters, the values in (10) and (11) give

$$\begin{aligned} Y_{f\pi\pi} &= \frac{Y_{f\pi N}^2}{Y_{fNN}} = 8.95 \pm 0.24 \text{ mb}, \\ Y_{\rho\pi\pi} &= \frac{Y_{\rho\pi N}^2}{Y_{\rho NN}} = 21.8 \pm 9.0 \text{ mb}. \end{aligned} \quad (18)$$

The phenomenological information about the coefficients  $Z$  and  $Y$  will be converted into standard Regge terminology in section 4.

### 3.4 Data on $\pi\pi$ cross sections

We complete this phenomenological discussion with a brief review of the experimental results for the  $\pi\pi$  total cross sections obtained indirectly, from reactions like  $\pi^- p \rightarrow \pi^+\pi^-n$ ,  $\pi^- p \rightarrow \pi^-\pi^-\Delta^{++}$  [7, 9, 10] and  $\pi^\pm p \rightarrow \Delta^{++}X$ ,  $\pi^\pm n \rightarrow pX$  [12, 13].

Fig. 1 shows that in the  $\pi^-\pi^+$  channel, the three available data sets [7, 9, 12] are more or less consistent, not only with one another, but also with the cross section that follows by applying factorization to the Regge representation in PDG 2011. The figure also indicates the cross section corresponding to some of the Regge representations available in the literature, as well as the outcome of our own analysis. These entries will be discussed in section 10.5.

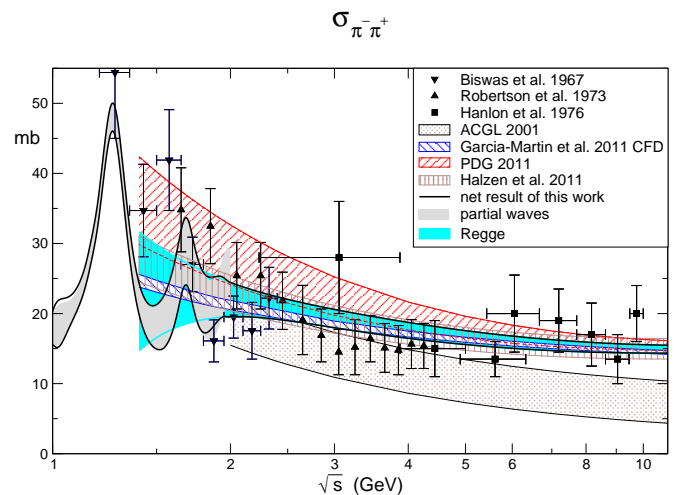


Fig. 1. Total  $\pi^-\pi^+$  cross section

In the channel  $\pi^-\pi^0$ , we are aware of only one set of data [7]. As these concern the region below 2 GeV, they do not contain information about the behaviour at high energies.

The  $\pi^-\pi^-$  channel does not contain resonances. At low energies, the cross section is small and notoriously difficult to measure. Various data are shown in Fig. 2. Those of Cohen et al. [10] concern the elastic rather than the total cross section. At low energies, however, the inelasticity in this channel is very small, so that the elastic cross section barely differs from the total one. In particular, the main source of inelasticity in  $\pi^-\pi^+$  collisions – transitions into  $K\bar{K}$  states – is forbidden here. This implies that the data of Biswas et al. [7] and Losty et al. [11] are in conflict with those of Cohen et al. [10]. Concerning the behaviour at higher energies, there is a clash between the data of Robertson et al. [9] and Abramowicz et al. [13]. Note that the energy range of this plot extends to 20 GeV, far beyond the region which matters in our context.

In the Regge parametrization of the  $\pi^-\pi^-$  cross section, the  $\rho$  contributes with a sign opposite to Pomeron and  $f$ . Since factorization determines the latter rather

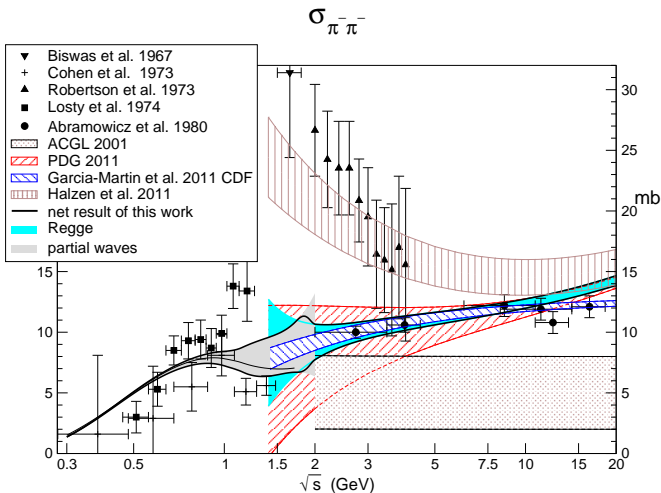


Fig. 2. Total  $\pi^-\pi^-$  cross section

sharply, the uncertainty of the result for  $\sigma_{\pi^-\pi^-}$  is dominated by the one in the residue of the Regge pole associated with the  $\rho$ . The red shaded area indicates the result obtained from  $\pi N$  and  $NN$  scattering with factorization, using equations (17) and (18). The uncertainty in this result is large, because (a) the  $\rho$  contribution to  $NN$  scattering is small and (b) the extraction of the  $\rho$  residue requires data on  $pn$  scattering, which are less precise. The other entries shown in the figure will be discussed in section 10.5.

## 4 Regge representation of the $\pi\pi$ amplitude

We now specify the parametrization of the  $\pi\pi$  scattering amplitude we are going to use at high energies. The dominant Regge poles with  $C = 1$  are the Pomeron and the  $f$ , while the channel with  $C = -1$  is dominated by the  $\rho$ -pole. What counts is the isospin in the  $t$ -channel. We use the notation<sup>3</sup> of reference [2], where the component of the scattering amplitude with  $t$ -channel isospin  $I_t$  is denoted by  $T^{(I_t)}(s, t)$ . In this notation, the optical theorem takes the form

$$\sigma^{(I_t)}(s) = \frac{\text{Im} T^{(I_t)}(s, 0)}{\sqrt{s(s - 4M_\pi^2)}}. \quad (19)$$

The Pomeron and the  $f$  contribute to  $T^{(0)}$  and  $\rho$  contributes to  $T^{(1)}$ , while the exotic amplitude  $T^{(2)}$  only receives subdominant contributions from the exchange of two or more Regge poles. In the dispersive framework we are using, the real parts are represented as dispersion integrals over the imaginary parts. As we are evaluating these integrals only at low energies, it suffices to specify the Regge representation of the imaginary parts – for the analysis of the Roy equations and sum rules discussed in

<sup>3</sup> In [32, 37] the scattering amplitude is instead denoted by  $F(s, t)$ . The normalization differs from ours by a numerical factor:  $T(s, t) = 4\pi^2 F(s, t)$ .

the present paper, the high energy behaviour of the real parts is not relevant.

The quantities  $\sigma_{\pi^\pm\pi^+}$ ,  $\sigma_{\pi^\pm\pi^0}(s)$  and  $\sigma_{\pi^0\pi^0}(s)$  represent linear combinations of the total cross sections of definite isospin in the  $t$  channel:

$$\begin{aligned} \sigma_{\pi^\pm\pi^+}(s) &= \frac{1}{3}\sigma^{(0)}(s) \mp \frac{1}{2}\sigma^{(1)}(s) + \frac{1}{6}\sigma^{(2)}(s), \\ \sigma_{\pi^\pm\pi^0}(s) &= \frac{1}{3}\sigma^{(0)}(s) - \frac{1}{3}\sigma^{(2)}(s), \\ \sigma_{\pi^0\pi^0}(s) &= \frac{1}{3}\sigma^{(0)}(s) + \frac{2}{3}\sigma^{(2)}(s). \end{aligned} \quad (20)$$

### 4.1 Parametrization of $\text{Im} T^{(0)}(s, t)$

Our explicit representation for the imaginary part of the component with  $I_t = 0$  reads:

$$\begin{aligned} \text{Im} T^{(0)}(s, t)_R &= \beta_P(t) \left(\frac{s}{s_1}\right)^{\alpha_P(t)} \times \\ &\left\{ 1 + \bar{B} \ln^2\left(\frac{s}{s_0}\right) + p_1 \frac{s_1}{s} \right\} + \beta_f(t) \left(\frac{s}{s_1}\right)^{\alpha_f(t)}, \end{aligned} \quad (21)$$

It contains the trajectories of Pomeron and  $f$ ,

$$\begin{aligned} \alpha_P(t) &= \alpha_P(0) + \alpha'_P(0)t, \\ \alpha_f(t) &= \alpha_f(0) + \alpha'_f(0)t. \end{aligned} \quad (22)$$

The range used for the intercepts and slopes is specified in equations (12)–(15).

We first comment on the coefficients relevant at  $t = 0$ , which govern the total cross section  $\sigma^{(0)}(s)$ . Using the optical theorem (19) on the right hand side of the first equation in (20) and comparing the result with (16), we obtain:

$$\begin{aligned} \beta_P(0) &= 3 s_1 Z_{\pi\pi} (\hbar c)^{-2} = 94 \pm 1, \\ \bar{B} &= B/Z_{\pi\pi} = 0.025 \pm 0.001, \\ \beta_f(0) &= 3 s_1 Y_{f\pi\pi} (\hbar c)^{-2} = 69 \pm 2, \end{aligned} \quad (23)$$

where we have explicitly indicated the conversion factor  $(\hbar c)^2 = 0.389 \text{ mb GeV}^2$  needed to arrive at dimensionless residues. As discussed in appendix A, the values of  $\beta_P(0)$  and  $\beta_f(0)$  proposed in the literature cover a large range. The relative weight of the contributions from the Pomeron and from the  $f$  depends on the parametrization chosen for the Pomeron. For our analysis, this does not present a significant source of uncertainty: the relative weight of the two contributions barely matters. It is important, however, that in the energy range of interest, factorization yields an unambiguous prediction for the sum of the two, that is for the total cross section with  $I_t = 0$ .

In (21), we have allowed for a pre-asymptotic contribution, whose size is determined by the coefficient  $p_1$ . The reason for including such a term is that we are making use of the parametrization in terms of Regge poles down to an energy of 1.7 GeV. The uncertainties in the residues given in (23) stem from an analysis of the observed  $\pi N$  and  $NN$  cross sections above 5 GeV. They do not cover the contributions generated by nonleading Regge poles, which

become increasingly important as the energy is lowered. In the representation (21), these contributions are modeled by a single term, which drops off more rapidly with the energy than the Pomeron, by one power of  $s$ .

We now turn to the  $t$ -dependence. While the term associated with the  $f$  is of the standard form of a Regge pole given in equation (1), the one describing the Pomeron contains the square of a logarithm. Following [63], we made the assumption that the Pomeron is a triple pole in the angular momentum plane, located at  $J = \alpha_P(t)$ . This is legitimate only if the energy is not too high. As pointed out in [76, 77], unitarity imposes a bound on the shape of the diffraction peak. The parametrization in (21) violates this bound at very high energies, for the following reason. In our normalization of the scattering amplitude, the differential cross section for elastic scattering reads

$$\frac{d\sigma}{dt} = \frac{|T(s, t)|^2}{16\pi s (s - 4M_\pi^2)}. \quad (24)$$

The contribution to this cross section from  $|\text{Im} T(s, t)|^2$  alone grows in proportion to  $\ln^4 s s^{2\alpha'_P(0)t}$ , so that the integral over  $t$  – the total elastic cross section – increases with the third power of  $\ln s$  and thus eventually becomes larger than the total cross section. The same problem also occurs if the intercept of the Pomeron is taken above unity,  $\alpha_P(0) > 1$ . There are well-known ways to avoid the clash with unitarity, for instance in Regge-eikonal models [67–70] valid at very high energies.

In the context of the present paper, the behaviour at very high energies is an academic issue, because the integrals over the Regge representation occurring in the evaluation of the various quantities of interest pick up significant contributions only from modest energies, where the logarithmic term represents a small, roughly energy independent correction. It could just as well be absorbed in the residue  $\beta_P(t)$  and in the sub-leading coefficient  $p_1$ , so that the problem would disappear. Nevertheless, a parametrization of the Pomeron that (i) reduces to the one used in the Review of Particle Properties [63] when  $t \rightarrow 0$  and (ii) is consistent with general principles also for large  $s$  and  $t \neq 0$  would be of considerable interest – we did not find such a representation in the literature.

We give the term proportional to  $p_1$  the same  $t$ -dependence as the Pomeron. This has the advantage that the pre-asymptotic contributions in the channel with  $I_t = 0$  are accounted for in terms of a single parameter, but it is evident that a simple parametrization of this sort can account for the nonleading terms only in a very crude way. Nevertheless, we will show that this parametrization allows us to make contact between the region where the first few partial waves represent a reliable approximation and the one where the amplitude can be represented in terms of a few Regge poles. The  $t$ -dependence of the residues  $\beta_P(t)$  and  $\beta_f(t)$  is discussed in section 11.

## 4.2 Parametrization of $\text{Im} T^{(1)}(s, t)$

For the component with  $I_t = 1$ , we work with the representation

$$\text{Im} T^{(1)}(s, t)_R = \beta_\rho(t) \left\{ 1 + r_1 \frac{s_1}{s} \right\} \left( \frac{s}{s_1} \right)^{\alpha_\rho(t)}. \quad (25)$$

It involves the  $\rho$ -trajectory,

$$\alpha_\rho(t) = \alpha_\rho(0) + \alpha'_\rho(0)t,$$

whose parameters are specified in (13) and (15), as well as a pre-asymptotic contribution, determined by the parameter  $r_1$ . For the interpretation of this term, we refer the reader to the last paragraph of the previous section – what we wrote for  $p_1$  also applies to  $r_1$ .

The result for the coefficient  $Y_{\rho\pi\pi}$  in (18), which follows from the Regge fits to the  $\pi N$  and  $NN$  data in [63], comes with a large uncertainty. The same applies to the corresponding result for the  $\rho$  residue at  $t = 0$ :

$$\beta_\rho(0) = 2 s_1 Y_{\rho\pi\pi} (\hbar c)^{-2} = 112 \pm 46. \quad (26)$$

In the following, we do not make use of this crude estimate. Instead, we rely on the determination of  $\beta_\rho(0)$  based on the Olsson sum rule [15], which will be discussed in section 10.2. Our determination is consistent with the above number, but somewhat more precise. The behaviour of  $\beta_\rho(t)$  at nonzero values of  $t$  is discussed in section 11.

## 4.3 Parametrization of $\text{Im} T^{(2)}(s, t)$

At the energies considered in the analysis of the high energy  $\pi N$  and  $NN$  data, contributions from exotic Regge channels are neglected. In the energy range discussed in the present paper, however, this is not justified. Indeed, as we will see, some of the sum rules obeyed by the scattering amplitude do require a small component with  $I_t = 2$ . In this channel, the dominating contributions stem from the exchange of two Regge poles with  $I_t = 1$ , so that the leading singularity in the angular momentum plane is a branch cut [21]. The leading contributions stem from  $\rho$ - $\rho$  and  $a_2$ - $a_2$  exchange. In the Regge representation we are using, which is based on [63], the  $a_2$  trajectory is taken degenerate with the  $f$ . Moreover, equations (13), (15) show that the  $f$  and  $\rho$  trajectories are rather close to one another: for the cut generated by  $\rho$ - $\rho$  exchange, the formula (4) gives  $\alpha_{\rho\rho}(0) = -0.10 \pm 0.04$  and  $\alpha'_{\rho\rho}(0) = 0.46 \pm 0.01$ , while the cut from  $f$ - $f$  exchange is characterized by  $\alpha_{ff}(0) = +0.08 \pm 0.10$ ,  $\alpha'_{ff}(0) = 0.50 \pm 0.08$ . Also, at the relatively low energies considered here, the neglected logarithms cannot be distinguished from the difference between  $\alpha_{\rho\rho}(0)$  and  $\alpha_{ff}(0)$ . The numerical values indicate that, compared to the dominating contribution from the Pomeron, the exotic component of the amplitude roughly falls off in proportion to  $1/s$ . The  $I_t = 2$  component of the scattering amplitude may thus be viewed like a pre-asymptotic contribution. We approximate it in the same

manner as the one occurring in the amplitude with  $I_t = 0$ , parametrizing it with a simple Regge pole,

$$\text{Im } T^{(2)}(s, t)_R = \beta_e(t) \left( \frac{s}{s_1} \right)^{\alpha_e(t)}, \quad (27)$$

where  $\beta_e(t)$  represents an effective residue and

$$\alpha_e(t) = \alpha_e(0) + \alpha'_e(0) t \quad (28)$$

is an effective trajectory with  $\alpha_e(0) = 0$ .

The formula (4) implies that the slope of the effective exotic trajectory is smaller than the slopes of the  $\rho$  or  $f$ -trajectories, by a factor of 2. This indicates that, compared to  $\rho$  and  $f$ , the relative importance of the exotic amplitude increases as one goes away from  $t = 0$ , towards spacelike values [61]. On the other hand, according to (14), the slope of the Pomeron trajectory is even smaller, so that, compared to the Pomeron, the exotic component loses weight if  $t$  becomes negative. We fix the exotic trajectory with

$$\alpha_e(0) = 0, \quad \alpha'_e(0) = 0.5 \pm 0.1 \text{ GeV}^{-2}. \quad (29)$$

The properties of the residue  $\beta_e(t)$  as a function of  $t$  are discussed in section 11.

## 5 Partial waves

The representation of the scattering amplitude in terms of Regge poles and cuts is dual to the one in terms of partial waves: the amplitude can be represented with either one of the two. We denote the partial wave amplitudes by  $t_\ell^I(s)$ , where  $I = 0, 1, 2$  stands for the  $s$ -channel isospin and  $\ell = 0, 1, 2 \dots$  denotes the angular momentum. We use the normalization

$$t_\ell^I(s) = \frac{1}{2i\rho(s)} \left\{ \eta_\ell^I(s) e^{2i\delta_\ell^I(s)} - 1 \right\}, \quad (30)$$

$$\rho(s) = \sqrt{1 - 4M_\pi^2/s},$$

where  $\eta_\ell^I(s)$  and  $\delta_\ell^I(s)$  denote the elasticity and the phase shift, respectively. The partial wave decomposition of the scattering amplitude then reads

$$T^I(s, t_z) = 32\pi \sum_\ell (2\ell + 1) P_\ell(z) t_\ell^I(s) \quad (31)$$

$$t_\ell^I(s) = \frac{1}{64\pi} \int_{-1}^{+1} dz P_\ell(z) T^I(s, t_z),$$

$$t_z = \frac{1}{2}(4M_\pi^2 - s)(1 - z),$$

where  $P_\ell(z)$  is the Legendre polynomial of order  $\ell$ . For the even angular momenta, Bose statistics permits  $I = 0$  and  $I = 2$ , while waves of odd angular momentum carry  $I = 1$ . We use the symbols  $S^0$  and  $S^2$  to distinguish the two S-waves, write  $P^1$  for the P-wave and label the higher partial waves analogously. In the region where the partial waves are small, the real and imaginary parts are approximately related by

$$\text{Im } t_\ell^I(s) \simeq \rho(s) \text{Re } t_\ell^I(s)^2 + \frac{1 - \eta_\ell^I(s)}{2\rho(s)}. \quad (32)$$

In this region, unitarity ( $0 \leq \eta_\ell^I(s) \leq 1$ ) sets a lower bound to the imaginary part, given by the first term in the above relation.

At low energies, the angular momentum barrier suppresses the contributions from high angular momenta. There, the decomposition of the amplitude into partial waves is preferable, because the first few terms in this decomposition suffice to obtain a decent approximation. At high energies, on the other hand, the Regge representation is more efficient, because the high energy behaviour of the amplitudes is dominated by the leading Regge poles. In the context of the present paper, which aims at an improved Regge parametrization, the partial wave representation plays an important role for two reasons: (i) We are making use of sum rules to analyze the  $t$ -dependence of the Regge residues. Since these involve integrals extending from threshold to infinity, we need an adequate representation also at low energies. (ii) The leading Regge poles yield a good approximation for the scattering amplitude only at very high energies. We need to bridge the gap between the region where the leading Regge poles dominate and the one where the Roy equations provide a reliable representation for the partial waves. Since the behaviour of the amplitudes between these two domains represents the main source of uncertainty in our analysis, we need to discuss it in some detail.

In the region where the Roy equations are valid, we determine the partial waves by solving these equations. The *input* of the calculation consists of four parts:

1. subtraction constants
2. elasticities below  $s_{max}$
3. partial wave imaginary parts above  $s_{max}$
4. driving terms

where  $\sqrt{s_{max}}$  is the upper end of the energy interval over which the equations are solved. In [2, 3], the upper end was taken at  $\sqrt{s_{max}} = 0.8 \text{ GeV}$  and the analysis was restricted to the S- and P-waves. In that case, the input unambiguously determines the solution. In the present paper, we consider the entire range where the Roy equations are valid, i.e. set  $\sqrt{s_{max}} = \sqrt{68} M_\pi \simeq 1.15 \text{ GeV}$ , and also calculate the D-, F- and G-waves. As discussed in detail in [2], the input listed above does then not determine the solution uniquely: on the extended interval, the Roy equations admit a 3-parameter family of solutions. We find it convenient to identify two of these degrees of freedom with the value of the  $S^0$  phase shift at two points in the interior of the interval on which we solve the Roy equations:  $\delta_0^0(s_A)$ ,  $\delta_0^0(4M_K^2)$ , with  $\sqrt{s_A} = 0.8 \text{ GeV}$ . The third one is fixed with the  $P^1$  phase shift:  $\delta_1^1(s_A)$ . The phenomenological estimates used for these quantities as well as those for the elasticities and for the imaginary parts of the partial waves are discussed in appendix B.3. The calculation of the driving terms is sketched in section 9.

Near threshold, the subtraction constants control the behaviour of the scattering amplitude. In the case of  $\pi\pi$  scattering, the dispersive representation involves two subtraction constants, which may be expressed in terms of the two S-wave scattering lengths,  $a_0^0$ ,  $a_0^2$ . At leading order of the chiral expansion, their values can be predicted

in terms of the pion decay constant [78]. The higher order corrections have been calculated in the framework of  $\chi$ PT [79, 80]. As pointed out in [3], the dispersive analysis of the scalar pion form factor [81] can be used to pin down one of the low energy constants occurring therein, so that a remarkably sharp theoretical prediction for the scattering lengths follows:

$$a_0^0 = 0.220 \pm 0.005, \quad a_0^2 = -0.0444 \pm 0.0010. \quad (33)$$

In the meantime, this prediction has been tested in a series of beautiful low energy precision experiments<sup>4</sup> concerning the decays  $K \rightarrow \ell\nu\pi\pi$  [83, 84],  $K \rightarrow \pi\pi\pi$  [85] and pionic atoms [86]. For the combination  $a_0^0 - a_0^2$ , where the experimental precision is comparable to the accuracy of the prediction, theory and experiment agree within errors. The data do not pin down the two individual scattering lengths to the same accuracy, but in combination with the fact that the dispersive evaluation of the scalar form factor leads to a sharp correlation between  $a_0^0$  and  $a_0^2$ , the experimental results imply  $a_0^0 = 0.2198(46)_{stat}(16)_{syst}(64)_{th}$ ,  $a_0^2 = -0.0445(11)_{stat}(4)_{syst}(8)_{th}$ , thus confirming the predictions to a remarkable degree of accuracy. Alternatively, as pointed out by Stern and collaborators [87], the two scattering lengths may be disentangled by invoking comparatively crude experimental results extracted from  $\pi N$  scattering. The recent update of this analysis by García-Martin et al. [37] leads to  $a_0^0 = 0.220(8)$ ,  $a_0^2 = -0.042(4)$ , also consistent with the predictions, albeit somewhat less precise.

Moreover, the recent progress made on the lattice now allows a calculation of  $a_0^2$  from first principles, analyzing the volume dependence of the energy levels of the system in a box of finite size [88–90]. Also, the low energy constants  $\bar{l}_3, \bar{l}_4$ , which dominate the uncertainties in the theoretical prediction for  $a_0^0$  and  $a_0^2$ , can now be determined on the lattice, from the dependence of  $M_\pi$  and  $F_\pi$  on the quark masses. The results are consistent with the estimates used in [3] and the uncertainties in  $\bar{l}_3$  are reduced significantly [91]. All of this corroborates the conclusion that the subtraction constants are reliably and accurately known. The remaining three parts of the input will be discussed below.

## 6 Partial wave representation of the total cross sections

In the present section, we briefly describe the qualitative picture obtained for the total cross sections, in order to set the stage for our analysis. The method used to derive this picture is outlined in section 9.

We denote the total cross sections with  $s$ -channel isospin  $I_s = 0, 1, 2$  by  $\sigma^0(s)$ ,  $\sigma^1(s)$ ,  $\sigma^2(s)$ , respectively. In this notation, the total cross sections for pions of definite charge are given by

$$\sigma_{\pi^+\pi^+}(s) = \sigma_{\pi^-\pi^-}(s) = \sigma^2(s), \quad (34)$$

<sup>4</sup> For recent reviews, we refer to [82].

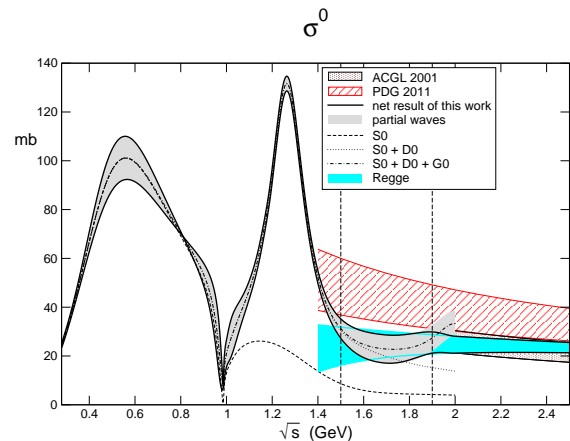


Fig. 3a Total  $\pi\pi$  cross section with  $I_s = 0$ .

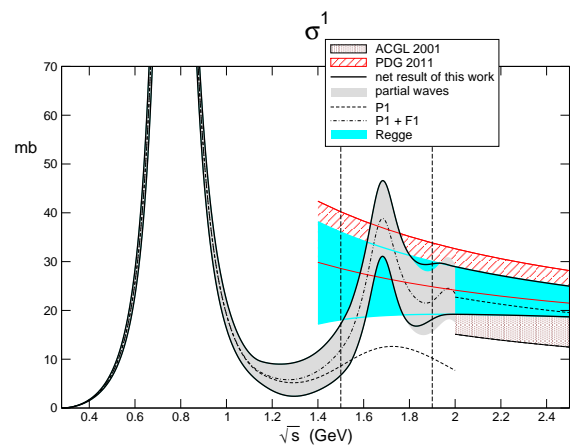


Fig. 3b Total  $\pi\pi$  cross section with  $I_s = 1$ .

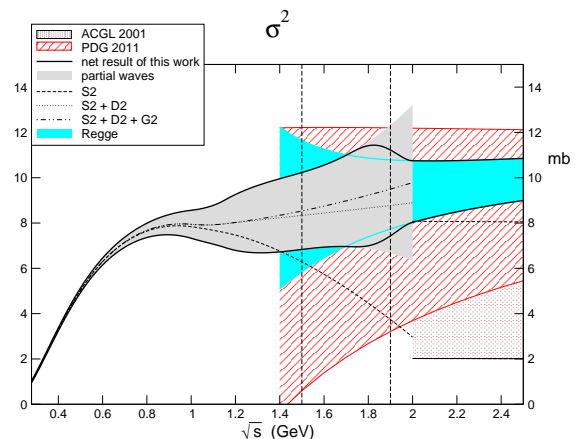


Fig. 3c Total  $\pi\pi$  cross section with  $I_s = 2$ .

$$\begin{aligned} \sigma_{\pi^-\pi^+}(s) &= \frac{1}{3}\sigma^0(s) + \frac{1}{2}\sigma^1(s) + \frac{1}{6}\sigma^2(s), \\ \sigma_{\pi^\pm\pi^0}(s) &= \frac{1}{2}\sigma^0(s) - \frac{1}{2}\sigma^2(s), \\ \sigma_{\pi^0\pi^0}(s) &= \frac{1}{3}\sigma^0(s) + \frac{2}{3}\sigma^2(s). \end{aligned}$$

The grey bands in Fig. 3 indicate our net result for the total cross sections obtained from the sum over the partial waves. The dashed black lines represent the central solutions of the Roy equations for the S- and P-waves. The



contributions from these waves dominate the total cross sections below 1 GeV, reach a maximum and then drop with the energy. The dotted black curves are obtained by adding the imaginary parts of the central Roy solution for  $D^0$  and  $D^2$ , respectively, while the dash-dotted ones include the F- and G-waves.

In the total cross section, the resonance peaks occurring in the imaginary parts of the individual partial waves generate an oscillatory behaviour, which only disappears gradually with increasing energy. Fig. 3a shows that, below 1 GeV,  $\sigma^0(s)$  is dominated by the contribution from the  $S^0$ -wave, which exhibits a broad bump around 600 MeV. The phenomenon reflects the presence of a pole on the second sheet of the partial wave amplitude  $t_0^0(s)$ , the well-known  $f_0(600)$  or  $\sigma$ . Slightly above 0.8 GeV, the phase shift passes through  $90^\circ$ . There, the inelasticity is very small, so that the  $S^0$ -wave nearly reaches the unitarity limit. This explains why the uncertainties in the total cross section are very small in that region. While the destructive interference with the  $f_0(980)$  generates a pronounced dip in the vicinity of  $K\bar{K}$  threshold, the behaviour between 1.15 and 1.5 GeV is dominated by the  $f_2(1275)$ . The contribution from the  $G^0$ -wave becomes visible only above 1.6 GeV. The first resonance with these quantum numbers, the  $f_4(2018)$ , can be seen, but it does not produce a marked peak, because many decay channels are open and the branching fraction  $\Gamma(f_4 \rightarrow \pi\pi)/\Gamma(f_4 \rightarrow \text{all})$  is below 20%.

The most prominent resonance, the  $\rho(770)$ , manifests itself in  $\sigma^1(s)$ . Since an appreciable inelasticity sets in only at  $M_\omega + M_\pi \simeq 0.92$  GeV, the contribution from the  $P^1$ -wave nearly saturates the unitarity limit at the peak of this resonance. The cross section  $\sigma^1(s)$  exceeds 220 mb there – the upper two thirds of the peak are chopped off, to make the behaviour of the cross section above 1 GeV more visible. The spin 3 resonance  $\rho_3(1690)$  produces a more modest peak, followed by an even weaker structure around 2 GeV. In the PDG listings, the lowest resonance with  $\ell = 5$  is the  $\rho_5(2330)$ . We expect partial waves with  $\ell > 4$  to play a significant role only above 2 GeV.

The exotic cross section  $\sigma^2(s) = \sigma_{\pi^-\pi^-}(s)$ , which does not receive contributions from resonances, is shown in Fig. 3c, a magnified version of Fig. 2. Below 1.15 GeV, the Roy equations provide good information about this cross section: they imply that the real parts of the exotic partial waves are dominated by the contributions from the imaginary parts of the non-exotic waves, which are known comparatively well. The uncertainties in  $\sigma^2(s)$ , however, grow with the energy – at  $\sqrt{s} = 2$  GeV, they are of order 3 mb.

Fig. 3 shows that, in the region between 1.5 and 2 GeV, our partial wave representations for the total cross sections with  $I_s = 0$  and  $I_s = 2$  are roughly energy independent, while the one with  $I_s = 1$  clearly reveals the presence of a resonance. Our quantitative estimates for the imaginary parts of the partial waves, which are outlined in appendix B.3, lead to substantial uncertainties in the total cross sections, which, moreover, grow with the energy – beyond 2 GeV, the partial wave decomposition is barely of practi-

cal use in our context. In the channels with  $I_s = 0$  or 1, the uncertainties mainly stem from the background underneath the resonances. In this language, the cross section in the channel with  $I_s = 2$  represents pure background. Indeed, Fig. 3 shows that our estimate for the uncertainties in  $\sigma^0(s)$  and  $\sigma^1(s)$  are comparable to the exotic total cross section  $\sigma^2(s)$ .

## 7 Duality

In the preceding sections, we discussed the Regge and partial wave representations by themselves. We now merge the two and first consider the forward direction,  $t = 0$ .

A simple way to join the two parametrizations of the imaginary parts is to use the partial wave representation below some energy  $E_t$  and the Regge representation above that energy. In order for the total cross sections not to make a jump at  $\sqrt{s} = E_t$ , the imaginary parts must be continuous there:

- In the case of  $\text{Im} T^{(0)}(s, 0)$ , this requirement can be used to fix the coefficient  $p_1$  of the pre-asymptotic term, so that, at  $t = 0$ , the Regge representation (21) does then not contain any unknowns: the total cross section  $\sigma^{(0)}(s)$  is determined also above the transition energy  $E_t$ .

- The Olsson sum rule subjects the cross section  $\sigma^{(1)}(s)$  to a constraint, which correlates the value of  $\beta_\rho(0)$  with the pre-asymptotic coefficient  $r_1$  (see section 10.2). Since the continuity requirement yields a second constraint of this type, we can determine  $\beta_\rho(0)$  as well as  $r_1$ . As a result, the total cross section is determined above  $E_t$ , also in the channel with  $I_t = 1$ .

- Finally, in the exotic  $t$ -channel, continuity determines the residue  $\beta_e(0)$  in terms of the partial wave representation at  $E_t$ , so that the Regge representation of  $\sigma^{(2)}(s)$  does then not contain any free parameters, either.

The choice of the transition energy represents a compromise: if  $E_t$  is taken too low, then our Regge representation does not provide a decent approximation, if it is taken too high, then our neglect of the partial waves with  $\ell > 4$  is not justified.

In [2–4], the transition from the partial wave representation to the Regge representation is made at 2 GeV, while in [32, 34–37] the Regge parametrization is assumed to be valid down to 1.42 GeV. The problem with the former analysis is that the phenomenological information used for the partial waves above 1.4 GeV leaves much to be desired, while the problem with the latter choice is that Regge asymptotics does not set in that early – see Fig. 3b.

Continuity may be viewed as a local version of duality: it requires the partial wave and Regge representations to agree at one particular energy. In the following, we use a weaker form of this requirement: we assume that the partial wave and Regge representations agree with one another only *in the mean*. For short, we refer to the resulting constraints as *duality conditions*.

More precisely, we replace the continuity conditions discussed above by the following constraints. Fig. 4 shows that the total cross sections with fixed  $t$ -channel isospin

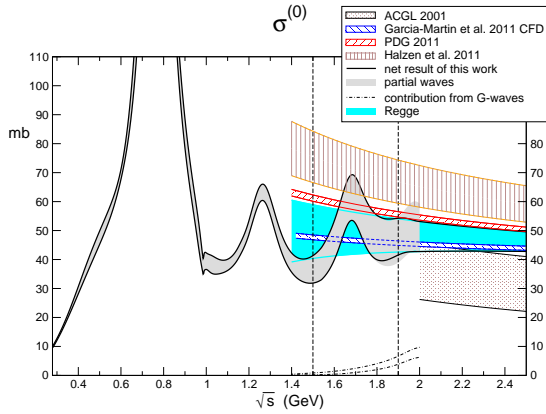


Fig. 4a Total  $\pi\pi$  cross section with  $I_t = 0$ .

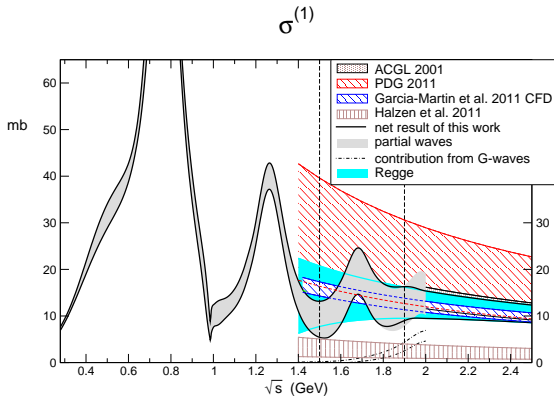


Fig. 4b Total  $\pi\pi$  cross section with  $I_t = 1$ .

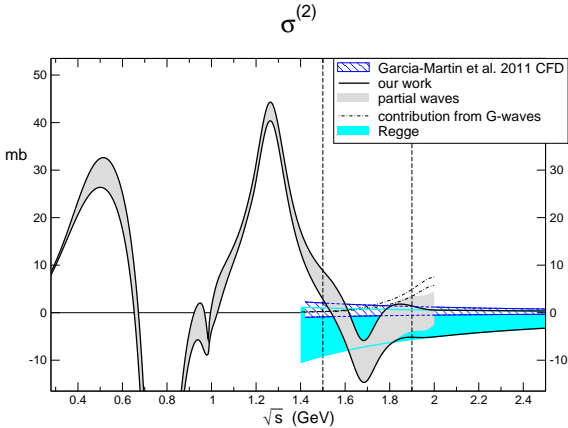


Fig. 4c Total  $\pi\pi$  cross section with  $I_t = 2$ .

$$\begin{aligned}\sigma^{(0)}(s) &= \frac{1}{3}\sigma^0(s) + \sigma^1(s) + \frac{5}{3}\sigma^2(s), \\ \sigma^{(1)}(s) &= \frac{1}{3}\sigma^0(s) + \frac{1}{2}\sigma^1(s) - \frac{5}{6}\sigma^2(s), \\ \sigma^{(2)}(s) &= \frac{1}{3}\sigma^0(s) - \frac{1}{2}\sigma^1(s) + \frac{1}{6}\sigma^2(s),\end{aligned}\quad (35)$$

either exhibit a peak or a dip, generated by the  $\rho(1690)$ . The dashed vertical lines indicate the adjacent valleys at 1.5 and 1.9 GeV, respectively. The bands labeled “Regge” are obtained by assuming that, on the interval spanned by these lines,  $1.5 \text{ GeV} < \sqrt{s} < 1.9 \text{ GeV}$ , the average over the partial wave representation of the total cross sec-

tions agrees with the average over the Regge representation. In other words, we assume that the inclusion of the pre-asymptotic terms allows us to extrapolate the Regge representation down to the above interval, not locally, but in the mean. Roughly, this amounts to imposing continuity at  $E_t$ , varying the value of  $E_t$  over the above range and averaging the result.

This version of duality lends itself to a natural generalization as well: it suffices to replace the total cross sections  $\sigma^{(k)}(s)$  by the functions  $\rho(s) \text{Im} T^{(k)}(s, t)$ . The duality conditions used in the present paper represent the requirement that the mean value of the Regge representation for these functions agrees with the partial wave representation thereof. Duality is useful in our framework, because it provides us with an estimate for the pre-asymptotic terms  $p_1, r_1, \beta_e(0)$ , much like the continuity conditions discussed above. Moreover, its generalization provides a constraint on the  $t$ -dependence of the Regge residues.

Whenever we calculate integrals over the imaginary parts of the  $\pi\pi$  amplitude we need to specify how the transition between the partial-wave and the Regge representation takes place. We assume that the partial wave representation provides an adequate approximation below 1.7 GeV and that the Regge representation yields an adequate approximation above 2 GeV. In the transition region, we use an interpolation,

$$\begin{aligned}\text{Im} T^{(I_t)}(s, t) &= \{1 - h(s)\} \text{Im} T^{(I_t)}(s, t)_{\text{PW}} \\ &+ h(s) \text{Im} T^{(I_t)}(s, t)_{\text{R}}, \quad s_a < s < s_b,\end{aligned}\quad (36)$$

with  $\sqrt{s_a} = 1.7 \text{ GeV}$ ,  $\sqrt{s_b} = 2 \text{ GeV}$ . The function  $h(s)$  interpolates between  $h(s_a) = 0$  and  $h(s_b) = 1$ . For definiteness, we take a cubic polynomial and fix the coefficients with the requirement that the first derivative is continuous at the lower and upper ends of the interpolation.<sup>5</sup> The interpolation (36) automatically ensures continuity, also at non-zero values of  $t$ .

## 8 Sum rules

The Olsson sum rule [15] originates in the fact that the  $t$ -channel  $I = 1$  amplitude does not receive a Pomeron contribution, and thus grows only in proportion to  $s^{\alpha_\rho(t)}$  for  $s \rightarrow \infty$ . The fixed- $t$  dispersion relation obeyed by this amplitude, however, does contain terms that grow linearly with  $s$ . For the relation to be consistent with Regge asymptotics, the contribution from the subtraction term must cancel the one from the dispersion integral. At  $t = 0$ , this condition reduces to a sum rule which expresses the combination  $2a_0^0 - 5a_0^2$  of the  $S$ -wave scattering lengths as an integral over the cross section  $\sigma^{(1)}(s)$  [15]:

$$2a_0^0 - 5a_0^2 = \frac{3M_\pi^2}{4\pi^2} \int_{4M_\pi^2}^{\infty} ds \frac{\sigma^{(1)}(s)}{\sqrt{s(s - 4M_\pi^2)}}. \quad (37)$$

The requirement that the amplitude  $T^{(1)}(s, t)$  has the proper high energy behaviour also for  $t \neq 0$  implies a

<sup>5</sup> The corresponding explicit expression for the interpolating function reads  $h(s) = (s - s_a)^2(3s_b - s_a - 2s)/(s_b - s_a)^3$ .

further constraint. This amplitude obeys the fixed- $t$  dispersion relation in equation (66) of appendix B.1. The constraint can be derived by evaluating the coefficient of the term on the r.h.s. of this equation that grows linearly with  $s$  and requiring that the term has the same value as for  $t = 0$ . This condition subjects the function  $\text{Im } T^{(1)}(s, t)$  to an entire family of sum rules of the form

$$S(t) = 0, \quad (38)$$

where  $t$  is a free parameter and the function  $S(t)$  is given by:

$$S(t) \equiv \frac{1}{\pi} \int_{4M_\pi^2}^{\infty} ds \frac{\text{Im } \bar{T}^{(1)}(s, t)}{s(s+t-4M_\pi^2)} - \frac{1}{\pi} \int_{4M_\pi^2}^{\infty} ds \frac{2(s-2M_\pi^2) \text{Im } T^1(s, 0)}{s(s-4M_\pi^2)(s-t)(s+t-4M_\pi^2)}. \quad (39)$$

The first integral involves only the  $I_t = 1$  component of the imaginary part. The bar indicates that the value at  $t = 0$  is subtracted:

$$\bar{T}(s, t) \equiv \frac{T(s, t) - T(s, 0)}{t}. \quad (40)$$

The function  $T^1(s, 0)$  in the second integral is the  $I_s = 1$  component at  $t = 0$ , which exclusively picks up contributions from partial waves of odd angular momentum. The integrand in (39) displays a fictitious pole for  $s = 4M_\pi^2 - t$ . However, for a crossing symmetric integrand, the residue of the pole vanishes. The sum rule  $S(t) = 0$  was written down already in [16] and was applied for the determination of the Regge residues in [17, 18]. For a detailed discussion, we refer to appendix C in [2].

The Roy equations are manifestly symmetric with respect to  $s \leftrightarrow u$ , but they do not ensure crossing symmetry with respect to  $s \leftrightarrow t$ , which requires the scattering amplitude  $\mathbf{T} = (T^0, T^1, T^2)$  to obey the relation

$$\mathbf{T}(s, t) - C_{st} \mathbf{T}(t, s) = 0. \quad (41)$$

On the other hand, any solution of the Roy equations that obeys this constraint is then automatically also crossing symmetric with respect to  $t \leftrightarrow u$ . Note that the subtraction constants as well as the contributions from the S- and P-waves drop out here: the relation (41) amounts to a family of sum rules that relate integrals over the imaginary parts of the partial waves with  $\ell \geq 2$  to integrals involving the Regge residues. We exploit these additional constraints by evaluating the derivative of (41) with respect to  $s$  at  $s = 0$ . As shown in appendix C, this leads to a new family of sum rules of the same type as the one above. We write these in the form  $C_k(t) = 0$ , with  $k = 0, 1, 2$ . Explicit expressions for the three functions  $C_0(t)$ ,  $C_1(t)$ ,  $C_2(t)$  are given in equation (75). As we will see, these sum rules provide us with a good tool to determine the  $t$ -dependence of the residues.

## 9 Method of analysis

Our analysis runs as follows:

1. We start with a complete representation of the amplitude, which specifies the imaginary parts of the partial waves below 2 GeV as well as the parameters occurring in the Regge representation.

2. As a first step, we calculate the driving terms for the partial waves with  $\ell \leq 4$ . The driving terms of a given wave consist of two parts: contribution from the imaginary parts of the other partial waves with  $\ell \leq 4$  below 2 GeV and contribution from all waves above 1.7 GeV. The former is smoothly cut off with the factor  $\{1 - h(s)\}$ , while the latter is gradually turned on with the factor  $h(s)$ , in accord with equation (36).

3. Next, we specify the input for which we wish to determine the full amplitude. Some of the input variables concern the partial wave representation, others concern the Regge parametrization. In fact, neither one of the two representations is fully specified by the input variables alone (see appendix B.3). We refer to the remaining parameters as output variables. The Roy equations determine the partial wave output, while the sum rules and duality conditions serve to determine the Regge output.

4. Together with the driving terms, the partial wave input uniquely determines the solution of the Roy equations. We solve these equations iteratively. The result is a new complete representation of the amplitude.

5. We then evaluate the various sum rules and duality conditions, which amount to constraints imposed on the Regge output variables. Since some of the sum rules and the duality conditions depend on  $t$ , we are in principle dealing with an infinite number of equations for a finite number of parameters and can therefore not expect to find an exact solution. Instead, we determine the minimum of a discrepancy function, obtained by adding up the various equations in quadrature – for details, we refer to appendix D. The minimum fixes the output variables of the Regge parametrization. In combination with the input specified in step 3, we thus arrive at a new Regge representation.

6. If the result of the preceding step differs significantly from the Regge representation we started with, we must return to step 2 and iterate the entire procedure. We find that the process converges rapidly – two or three iterations suffice to arrive at a self-consistent solution of good quality.

7. For a given choice of the input, the above procedure provides us with a complete representation of the amplitude. We finally need to determine the response of the output to changes in the input. As the variations of interest are small, the result for the partial wave and Regge representations of the scattering amplitude is approximately linear in these variations. We treat the input parameters as independent Gaussian variables, with one exception: we account for the correlation<sup>6</sup> between the two scattering lengths  $a_0^0$  and  $a_0^2$ . The error analysis is then straightforward.

<sup>6</sup> This correlation cannot be ignored; the error in the combination  $2a_0^0 - 5a_0^2$ , for instance, which plays a prominent role in the Olsson sum rule, is significantly smaller than what is obtained if the two terms are treated as independent.

ward – the quantities of interest are linear functions of the input variables and we can calculate the uncertainties therein as well as the correlations between them by averaging over the Gaussian fluctuations in these variables.

## 10 Regge analysis of the total cross sections

### 10.1 Total cross section with $I_t = 0$

We first illustrate the method with the determination of the pre-asymptotic coefficient  $p_1$ . As discussed in section 3, factorization yields a rather sharp prediction for the asymptotic behaviour of the total  $\pi\pi$  cross section in the channel with  $I_t = 0$ . The prediction is shown as a narrow red band in Fig. 4a, obtained by inserting the values (23) for  $\beta_P(0)$  and  $\beta_f(0)$  in the formula (21), setting the pre-asymptotic coefficient  $p_1$  equal to zero and calculating the corresponding cross section with the optical theorem (19).

Since the grey band in Fig. 4a, which represents the partial wave representation of the cross section  $\sigma^{(0)}(s)$ , passes below the extrapolation of the contributions from  $\beta_P(0)$  and  $\beta_f(0)$ , the pre-asymptotic term must be negative. The numerical evaluation of the duality condition formulated above implies that the coefficient  $p_1$  is in the range

$$p_1 = -0.8 \pm 0.6. \quad (42)$$

### 10.2 Olsson sum rule

The analysis of the total cross section in the channel with  $I_t = 1$  is more involved, because we do not make use of the result obtained from the  $\pi N$ ,  $NN$  and  $\bar{N}N$  data with factorization. As discussed in section 4.2, the error bar in that result is rather large. We instead rely on the Olsson sum rule (37), which states that an integral over the cross section  $\sigma^{(1)}(s)$  is determined by a combination of S-wave scattering lengths. The l.h.s. is known from  $\chi$ PT [3]:

$$2a_0^0 - 5a_0^2 = 0.663 \pm 0.007. \quad (43)$$

The prediction is very sharp, because the NLO corrections to Weinberg’s low energy theorem [78] exclusively involve the low energy constant  $\ell_4$  [79]. Chiral symmetry implies that the same constant also governs the chiral expansion of the scalar radius of the pion. The value quoted in (43) relies on a dispersive calculation of the scalar pion form factor [81] and accounts for all contributions up to and including NNLO of the chiral expansion [80]. As discussed in section 5, the predictions for the scattering lengths have in the meantime been corroborated, both experimentally and on the lattice. Concerning the specific combination relevant for the Olsson sum rule, the “best value” obtained on the basis of the available experimental information in [37] is  $2a_0^0 - 5a_0^2 = 0.650 \pm 0.015$ , thus confirming the prediction (43) to an accuracy of 2.5%.

The integral on the r.h.s. of (37) can be evaluated with the optical theorem (19). Below 1.7 GeV, the integrand is represented as a sum over the partial waves discussed in

section 5, while above 2 GeV, the Regge representation in (25) is relevant. In the transition region, we are using the interpolation (36). The Olsson integral is then given by the sum of two terms:  $O = O_{\text{PW}} + O_{\text{R}}$ , with

$$O_{\text{PW}} \equiv \frac{3M_\pi^2}{4\pi^2} \int_{4M_\pi^2}^{\infty} ds \frac{1-h(s)}{\sqrt{s(s-4M_\pi^2)}} \sigma_{\text{PW}}^{(1)}(s), \quad (44)$$

$$O_{\text{R}} \equiv \frac{3M_\pi^2}{4\pi^2} \int_{4M_\pi^2}^{\infty} ds \frac{h(s)}{\sqrt{s(s-4M_\pi^2)}} \sigma_{\text{R}}^{(1)}(s).$$

Below 1.15 GeV, we solve the Roy equations for the S, P, D, F and G partial waves. From there to 2 GeV, we use a parametrization based on phenomenology (see appendix B.3). Table 1 lists the numerical results obtained for the contributions from the partial waves considered. The table

$S^0$	$0.315_{-0.011}^{+0.019}$
$S^2$	$-0.078_{-0.005}^{+0.007}$
$P^1$	$0.246_{-0.019}^{+0.017}$
$D^0$	$0.061 \pm 0.003$
$D^2$	$-0.007 \pm 0.003$
$F^1$	$0.013 \pm 0.001$
$G^0$	$0.0021 \pm 0.0003$
$G^2$	$-0.0007 \pm 0.0007$
$O_{\text{PW}}$	$0.552_{-0.016}^{+0.022}$

**Table 1.** Partial wave contributions to the Olsson sum rule.

shows that the result is dominated by the contributions from  $S^0$  and  $P^1$ . The uncertainties in the contributions from the partial waves are not symmetric, because the input used for the value of the phase shift  $\delta_0^0$  at 0.8 GeV is asymmetric (see appendix B.3).

Note that the errors are correlated – the uncertainty attached to the sum given at the bottom of the table is smaller than what is obtained by summing the individual errors in quadrature, because it accounts for the correlations. These also need to be accounted for when evaluating the combination

$$\bar{O}_{\text{PW}} \equiv O_{\text{PW}} - 2a_0^0 + 5a_0^2 : \quad (45)$$

since the values of the scattering lengths enter the Roy solutions, the term  $O_{\text{PW}}$  depends on these. The net result reads

$$\bar{O}_{\text{PW}} = -0.110_{-0.015}^{+0.022}. \quad (46)$$

### 10.3 Total cross section with $I_t = 1$

In the above notation, the Olsson sum rule amounts to the relation  $\bar{O}_{\text{PW}} + O_{\text{R}} = 0$ . Since the representation (25) for  $\text{Im} T^{(1)}(s, t)$  is proportional to the residue of the Regge pole with the quantum numbers of the  $\rho$ , the cross section  $\sigma_{\text{R}}^{(1)}(s)$  is proportional to  $\beta_\rho(0)$  and in addition involves the coefficient  $r_1$  of the pre-asymptotic term, as well as the intercept of the  $\rho$ -trajectory,  $\alpha_\rho(0)$ . Actually, in the

narrow range (13) we adopt for this intercept, the integral is not sensitive to  $\alpha_\rho(0)$ . Evaluating it with the central value, the result (46) implies

$$\beta_\rho(0)(1 + 0.104 r_1) = 80_{-16}^{+11}. \quad (47)$$

The Olsson sum rule thus leads to a linear correlation be-

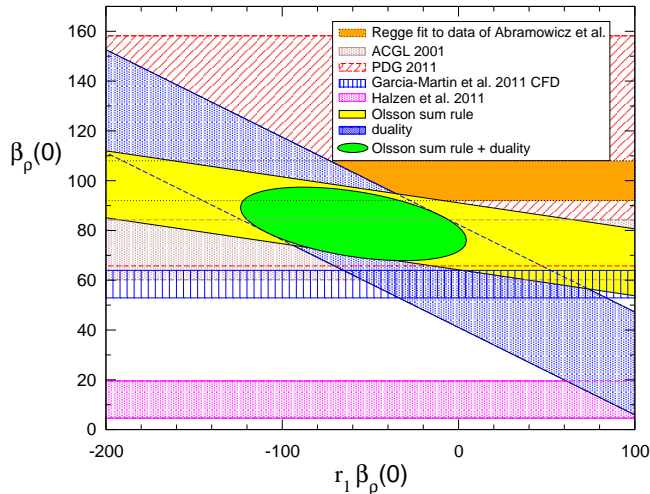


**Fig. 5.** Regge term with the quantum numbers of the  $\rho$ . The constraints imposed by the Olsson sum rule and by duality are compared with the results for  $\beta_\rho(s)$  obtained from other sources: Regge parametrization quoted in the Review of Particle Properties [63] plus factorization; fit to the data of Abramowicz et al. [13]; various values taken from the literature [2], [37], [74]. The ellipse represents the result of our analysis in equation (49).

tween  $\beta_\rho(0)$  and  $r_1\beta_\rho(0)$ , which is indicated by the yellow band in Fig. 5. Because of the linearity, the error analysis simplifies considerably if the variable  $r_1$  is replaced by  $r_1\beta_\rho(0)$  and we will do that.

The duality condition, which requires that, on the interval  $1.5 \text{ GeV} < \sqrt{s} < 1.9 \text{ GeV}$ , the average over the partial wave representation agrees with the average over the Regge representation yields a second relation of this form:

$$\beta_\rho(0)(1 + 0.351 r_1) = 61_{-9}^{+10}. \quad (48)$$

In Fig. 5, this constraint is shown as a blue band.

The right hand sides of (47) and (48) are obtained by averaging over the uncertainties attached to the Roy solutions and are therefore correlated. In order to account for these correlations as well as for the uncertainties in  $\alpha_\rho(0)$ , we use the method outlined in section 9 and calculate the central values and the correlation matrix of the two quantities  $\beta_\rho(0)$  and  $r_1\beta_\rho(0)$ . The ellipse shown in Fig. 5 indicates the corresponding  $1 \sigma$  contour and represents our final result for these two quantities. While the bands do not account for the correlation between the r.h.s. of (47) and (48), the ellipse does – this is the main reason why the bands are not exactly tangent to the ellipse (the remaining difference stems from the fact that the ellipse also

accounts for the uncertainty in  $\alpha_\rho(0)$ , while the bands do not). Expressed in terms of the two original parameters  $\beta_\rho(0)$  and  $r_1$ , our result reads:

$$\beta_\rho(0) = 84_{-16}^{+13}, \quad r_1 = -0.8_{-0.7}^{+0.8}. \quad (49)$$

There is a modest correlation between these two variables; the correlation coefficient is  $-0.33$ . The result for  $\beta_\rho(0)$  will be compared with values found in the literature in section 10.5.

#### 10.4 Total cross section with $I_t = 2$

The analysis of the total cross section with isospin 2 in the  $t$ -channel closely parallels the one in section 10.1. The grey band in Fig. 4c indicates the sum of the partial waves for the corresponding total cross section. The resonances are seen clearly, because  $\sigma^{(2)}(s)$  is not positive and the resonance contributions alternate in sign. The last resonance seen is the  $\rho_3(1690)$  which generates a small dip.

The high energy behaviour is parametrized with the expression (27). According to (29), the total cross section falls approximately in inverse proportion to  $s$ . In this channel, the requirement that, on the interval between 1.5 and 1.9 GeV, the average over the partial wave representation agrees with the average over the Regge representation implies

$$\beta_e(0) = -24 \pm 29. \quad (50)$$

#### 10.5 Discussion: total cross sections

The Regge parameters emerging from our analysis at  $t = 0$  are given in equations (23), (42) for  $I_t = 0$ , in (49) for  $I_t = 1$ , and in (50) for  $I_t = 2$ . The final result for the total cross sections, obtained with the interpolation described in section 7, is shown as a solid line in Figs. 1–4.

An important feature of our representation is the presence of pre-asymptotic terms. As mentioned above, such terms become relevant if the Regge representation is used at relatively low energies. In the following sections, we will show that the semi-local form of duality invoked in the present paper does lead to a coherent picture, provided the pre-asymptotic contributions are accounted for. We emphasize, however, that the simple parametrization used for these terms can only give a very rough description of the contributions occurring underneath the leading Regge poles.

In the cross section with  $I_t = 0$ , the estimate (42) for the pre-asymptotic term reduces the contribution from Pomeron and  $f$  at 2 GeV by  $20 \pm 15\%$ . Fig. 4a shows that, towards lower energies, this term widens the band spanned by the Regge representation, leaving room for resonances. Towards higher energies, the pre-asymptotic contribution shrinks. At 5 GeV (lower end of the energy range used for the Regge analysis of the  $\pi N$  and  $NN$  data in [63]), it amounts to  $3 \pm 2\%$ .

Our estimate (49) for the pre-asymptotic term in the channel with  $I_t = 1$  is consistent with zero. The main

effect of this term is to increase the uncertainties in the result obtained for the Regge parametrization at low energies. Non-leading contributions of this size generate sufficient broadening, so that the extrapolation below 2 GeV becomes consistent with the representation in terms of partial waves, at least in the average sense. Note that in the channel with  $I_t = 1$ , the resonances generate more pronounced fluctuations than for  $I_t = 0$ , because the constant background related to the Pomeron is missing here: between 1.3 and 1.5 GeV, the sum of the partial wave contributions drops from  $34 \pm 2$  to  $7 \pm 3$  mb and then again increases to  $14 \pm 4$  mb when the energy reaches 1.7 GeV.

The entire component of the Regge representation with  $I_t = 2$  amounts to a pre-asymptotic contribution. The result given in (50) shows that, at  $t = 0$ , this term vanishes within errors. The corresponding total cross section is in the range  $\sigma^{(2)}(2 \text{ GeV}) = -2 \pm 3$  mb, small compared to the leading cross section  $\sigma^{(0)}(2 \text{ GeV}) = 48 \pm 5$  mb, which is dominated by the contribution from the Pomeron.

We conclude that the Regge representation exhibits the expected qualitative features already at 2 GeV. Our results are in general agreement with the total  $\pi^-\pi^+$  cross section data shown in Fig. 1, while among the  $\pi^-\pi^-$  data above 1.5 GeV shown in Fig. 2, only those of Abramowicz et al. are consistent with our framework. In fact, these data provide an independent estimate for the size of the coefficient  $Y_{\rho\pi\pi}$  in the Regge formula (16) for the total  $\pi\pi$  cross section. Taking the values of the coefficients  $B, s_0, Z_{\pi\pi}, Y_{f\pi\pi}$  from factorization, neglecting contributions with  $I_t = 2$  as well as pre-asymptotic terms, and treating  $Y_{\rho\pi\pi}$  as a free parameter, we obtain an acceptable fit to the data of Abramowicz et al. [13], with  $\chi^2 = 7.7$ , for 5 degrees of freedom and  $Y_{\rho\pi\pi} = 19.5 \pm 1.6$  mb. This corresponds to  $\beta_\rho(0) = 100 \pm 8$ , consistent with (49), as seen also from Fig. 5.

It can be further checked that the pre-asymptotic terms do not distort the description at the energies where the data of Abramowicz et al. were taken. Evaluating  $\chi^2$  with the results obtained for  $p_1, \beta_e(0), \beta_\rho(0)$  and  $r_1$  in (42), (50), (49), and accounting for the correlations among these variables, we obtain  $\chi^2 = 6.8$  for 6 data points, no free parameters. As compared to the fit mentioned above, the quality thus even improves a little. We conclude that the results obtained above for the non-leading Regge contributions at  $t = 0$  are perfectly consistent with the data of Abramowicz et al.

Figs. 1–4 also show several other Regge parametrizations of the  $\pi\pi$  amplitude at high energies. The red bands indicated as PDG 2011 in Figs. 3a–c and 4a, 4b are based on the results given in equations (23) and (26), which are obtained from the  $\pi N, NN$  and  $\bar{N}N$  data above 5 GeV with factorization. As discussed in section 4.2, the large width of these bands in Figs. 3 and 4b is due to the poor extraction of  $\beta_\rho(0)$ . The central value of the factorization estimate for  $\beta_\rho(0)$  is on the high side, but in view of its large error bar it is consistent with the value (49), extracted from totally independent information.

The Roy equation analysis performed in [2, 3] is based on Pennington's representation [21]. The bands denoted

as ACGL 2001 in Figs. 3 and 4 show that the Pomeron estimate used in [2],  $\beta_P(0) = 46 \pm 38$ , although equipped with a large error, is too low. On the other hand, our analysis does confirm the value  $\beta_\rho(0) = 72$  given in [21] and adopted in [2]. As noted in [3], this result is perfectly consistent with the theoretical prediction for the combination  $2a_0^0 - 5a_0^2$  of scattering lengths that is relevant for the Olsson sum rule.

The hatched bands that extend down to 1.42 GeV indicate the Regge representation labeled CFD in [37], which corresponds to  $\beta_P(0) = 98.7 \pm 1.6$ ,  $\beta_f(0) = 31.6 \pm 1.9$ ,  $\beta_\rho(0) = 58.4 \pm 5.5$  and  $\beta_e(0) = 3.15 \pm 7.9$ . The corresponding trajectories, as well as the results for the residues obtained in the previous works of the same authors, are quoted in appendix A. We note that, although the values of the  $f$  and  $\rho$  residues are smaller than our results in (23) and (49), the Regge representation for the total cross section with  $I_t = 0$  and  $I_t = 1$  given in [37] is consistent with ours. The reason is the presence of the pre-asymptotic terms in our amplitudes, which are negative and in effect reduce the contributions from the dominant residues. The larger intercepts of the  $f$  and  $\rho$  trajectories adopted in [37] also count: at 2 GeV, for instance, with the value  $\alpha_\rho(0) = 0.53$  adopted in [37], the factor  $s^{\alpha_\rho}$  is larger by 10% than the same factor calculated with our value (13). As concerns the overall behaviour of the cross sections above 1.7 GeV, the representation given in [37] is consistent with ours.

Factorization is exploited also in a very recent analysis<sup>7</sup> of the hadronic cross sections by Halzen et al. [74], which leads to a value  $Z_{\pi\pi} = (12.7 \pm 1.4)$  mb consistent with (17), but a higher  $Y_{f\pi\pi} = (16.0 \pm 3.9)$  mb and a lower  $Y_{\rho\pi\pi} = 1.9_{-1.0}^{+1.9}$  mb, compared with the numbers in (18). These discrepancies originate in the fact that the authors of [74] use a small coupling  $Y_{fNN}$ , and a large coupling  $Y_{\rho NN}$  in the denominator of the factorization relations (18). Actually, the values of  $Y_{1pp}$  and  $Y_{2pp}$  obtained in [74] by independent fits of  $pp$  forward scattering data, including the total cross section at 7 TeV measured recently at LHC, are not very different from those given in PDG 2011 and quoted in equation (9). But the individual contributions of the trajectories are then separated assuming the equalities  $Y_{fNN} = Y_{a_2NN}$  and  $Y_{\rho NN} = Y_{\omega NN}$ . The values reported in equation (10) and the discussion below it show that this assumption is strongly violated. As seen from Figs. 4a, 4b and 5, the unusual Regge picture of the  $\pi\pi$  cross sections proposed in [74] is in conflict with our analysis.

Finally, we consider the so-called exchange degeneracy, which requires  $\alpha_f(t) = \alpha_\rho(t)$  and  $\beta_f(t) = 3/2\beta_\rho(t)$ . In the Lovelace-Shapiro-Veneziano model [14], these relations indeed follow from the absence of exotic resonances.

<sup>7</sup> Footnote added in August 2012. The comments made in this paragraph concern a preliminary version of reference [74], available at <http://arxiv.org/abs/1110.1479v1>. In the published version of that paper, which recently appeared in Phys. Rev. D85 (2012) 074020, the deficiency is taken care of. The new values for the residues  $Y_{f\pi\pi} = (11.5 \pm 0.9)$  mb and  $Y_{\rho\pi\pi} = (19 \pm 5)$  mb are consistent with our estimates.

In contrast to other analyses, [2] for instance, we do not assume exchange degeneracy to hold, and it turns out that our results for  $\beta_f(0)$  and  $\beta_\rho(0)$  given in (23) and (49), respectively, do not have this property. However, as emphasized below equation (23), only the sum of the contributions from Pomeron and  $f$  counts, so that the value of  $\beta_f(0)$  is sensitive to the chosen parametrization. To illustrate this point, we mention that the parametrization of the total  $NN$  and  $\pi N$  cross section adopted by PDG before 2002 [58] leads via factorization to the values  $\beta_P(0) = 57 \pm 1$ ,  $\beta_f(0) = 111 \pm 2$ ,  $\beta_\rho(0) = 82 \pm 15$ , which happen to be consistent with exchange degeneracy. We conclude that, within our framework, the residue  $\beta_f(t)$  is too sensitive to the parametrization used for the Pomeron to give an unambiguous answer to the question of whether or not the residues of  $\rho$  and  $f$  are approximately exchange degenerate.

## 11 Regge analysis for $t \neq 0$

### 11.1 $t$ -dependence of the residues

The status of the Regge representation for amplitudes at nonzero momentum transfer is more uncertain than that for the total cross sections. Several global Regge fits of data on soft hadronic processes, available in the early literature [46], [47], [53] are in rough agreement, but disagree on details. The absorption corrections, which are large for nonforward scattering, are expected to change the residues of the pure Regge poles. Since these corrections are in general process-dependent, they can violate factorization [21], [51]. We mention also the more recent analysis reported in [71]. However, a systematic treatment of all the data sets for  $t \neq 0$  is not yet available.

The representations (21), (25), (27) leave the  $t$ -dependence of the Regge representation for the imaginary parts open. In order to complete our parametrization, we need to specify the dependence of the residues  $\beta_P(t)$ ,  $\beta_f(t)$ ,  $\beta_\rho(t)$ ,  $\beta_e(t)$  on the variable  $t$ . It is convenient to factor out the value at  $t = 0$ :

$$\beta_k(t) = \beta_k(0) \bar{\beta}_k(t), \quad k = P, f, \rho, e. \quad (51)$$

We refer to the functions  $\bar{\beta}_k(t)$  as *profiles*.

In the framework of the Roy equations, we are interested in the range  $-32M_\pi^2 < t < 4M_\pi^2$ , where Mandelstam analyticity implies that fixed  $t$  dispersion relations hold in the interval  $-4M_\pi^2 < s < 68M_\pi^2 \simeq (1.15 \text{ GeV})^2$ . Numerically, the range of interest for the variable  $t$  corresponds to  $-0.62 \text{ GeV}^2 < t < 0.08 \text{ GeV}^2$ .

In the following, we exploit the fact that the sum rules strongly correlate the  $t$ -dependence of the Regge residues with the  $t$ -dependence of the partial waves. In fact, these sum rules can be solved for  $\bar{\beta}_P(t)$ ,  $\bar{\beta}_\rho(t)$ ,  $\bar{\beta}_e(t)$ . The results are of the same accuracy as those for the residues at  $t = 0$ , because the uncertainties in the  $t$ -dependence originate in the same sources.

The fourth profile,  $\bar{\beta}_f(t)$ , cannot be determined in this way, because the sum rules only concern the sum of Pomeron and  $f$  and do not allow us to clearly separate the two

contributions. For the same reason, however, the specific form used for  $\bar{\beta}_f(t)$  is not crucial.

The discussion below equation (2) imposes an important constraint on  $\bar{\beta}_f(t)$ . The  $f$  is even under charge conjugation,  $\tau_f = 1$ . Hence the absence of ghosts implies that  $\bar{\beta}_f(t)$  must vanish at the place where the trajectory  $\alpha_f(t)$  passes through zero. This happens around  $t \simeq -0.6 \text{ GeV}^2$ , that is, within the  $t$ -interval of interest, close to the lower end. The condition leaves little freedom in the  $t$ -dependence of this residue. We neglect the curvature and approximate it with a straight line,  $\bar{\beta}_f(t) \propto \alpha_f(t)$ , so that the profile is given by:

$$\bar{\beta}_f(t) = 1 + b_f t, \quad b_f = \frac{\alpha_f'(0)}{\alpha_f(0)}. \quad (52)$$

Fig. 6 visualizes this approximation: the area spanned

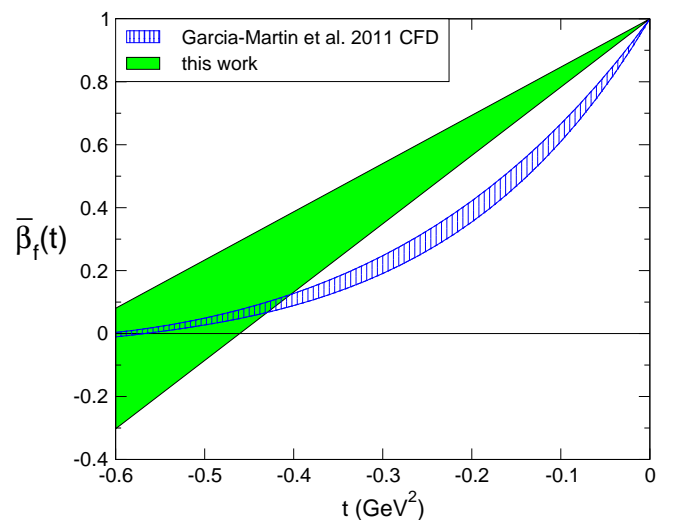


Fig. 6. Profile of the  $f$  residue.

by the full band corresponds to the uncertainty range in (13) and (15). We can allow for a curvature term – the sum rules then yield a somewhat different profile for the Pomeron. We have checked that, as long as the curvature is not larger than in the other residues, it barely affects our results. For comparison, the figure also shows the profile of the analogous term in the Regge parametrization of [37], where the symbol  $P'$  is used instead of  $f$ .

Concerning the approximation used for the remaining three profiles, the situation is the same as with the parametrization of the phase shifts used when solving the Roy equations: since the sum rules allow us to calculate these, the parametrization of the profiles is a mere matter of convenience. We find that, on the domain of interest to us,  $-0.62 \text{ GeV}^2 \leq t \leq 0$ , a parabolic parametrization is adequate:

$$\bar{\beta}_k(t) = 1 + b_k t + c_k t^2, \quad k = P, f, \rho, e. \quad (53)$$

The accuracy to which the sum rules and duality conditions are obeyed does improve a little if we allow for

cubic or quartic terms, but the results can barely be distinguished from those obtained with (53). In this notation, the representation (52) for  $\bar{\beta}_f(t)$  amounts to  $c_f = 0$  and the numerical values for intercept and slope of the  $f$ -trajectory in (13) and (15) imply

$$b_f = 1.7 \pm 0.3 \text{ GeV}^{-2}. \quad (54)$$

As we will see, the central solution for  $\bar{\beta}_\rho(t)$  also contains a zero, not far from the one in  $\bar{\beta}_f(t)$ . This phenomenon, however, is not related to the absence of a ghost. Since the  $\rho$  is odd under charge conjugation,  $\tau_\rho = -1$ , the absence of ghosts calls for a zero in  $\bar{\beta}_\rho(t)$  at the value of  $t$  where  $\alpha_\rho(t)$  passes through  $-1$ . As this happens near  $t \simeq -1.6 \text{ GeV}^2$ , far outside the range of interest, the condition that  $\bar{\beta}_\rho(t)$  must vanish there does not impose a significant constraint on our analysis (incidentally, the parabolic parametrization (53) of our central solution does contain a second zero at large negative values of  $t$ , but it occurs outside the region where that parametrization is relevant).

## 11.2 Profile of the Pomeron

The green band in Fig. 7 shows the outcome of our calculation for the  $t$ -dependence of the Pomeron residue. Numerically, the upper and lower edges of the band can be represented as  $\bar{\beta}_P(t) \pm \delta\bar{\beta}_P(t)$ , with<sup>8</sup>

$$\begin{aligned} \bar{\beta}_P(t) &= 1 + 2.24t + 1.76t^2, \\ \delta\bar{\beta}_P(t) &= 0.36t + 0.26t^2. \end{aligned} \quad (55)$$

For the slope at  $t = 0$ , the calculation yields:<sup>9</sup>

$$b_P = 2.5 \pm 0.4 \text{ GeV}^{-2}. \quad (56)$$

The figure shows that the sum rule analysis confirms the description of the Pomeron profile in terms of the e.m. form factor of the pion,

$$\bar{\beta}_P(t) = F_\pi(t)^2, \quad (57)$$

which was introduced by Donnachie and Landshoff [54] and adopted in [60, 61, 67]: the dash-dotted line shows the profile obtained from this formula with vector meson dominance, which predicts  $F_\pi(t) = 1/(1 - t/M^2)$ ,  $M = M_\rho$ . A parametrization of this form is used also by Cudell et al. [71], but the resulting picture is qualitatively different from the one in [54]: the estimate for the parameter  $M$  resulting from the fits constructed in [71] is more than twice as large as  $M_\rho$ , so that the Pomeron profile falls off

<sup>8</sup> Throughout, the coefficients occurring in the polynomial representations of the residues as well as the slope parameters  $b_P, b_f, b_\rho, b_e$  and  $\beta'_e(0)$  are given in  $\text{GeV}$  units.

<sup>9</sup> The value given for  $b_P$  agrees with  $\bar{\beta}'_P(0) \pm \delta\bar{\beta}'_P(0)$  only roughly: the former involves the square root of a sum of squares of the derivative while the latter is obtained by taking the derivative of a square root of a sum of squares.

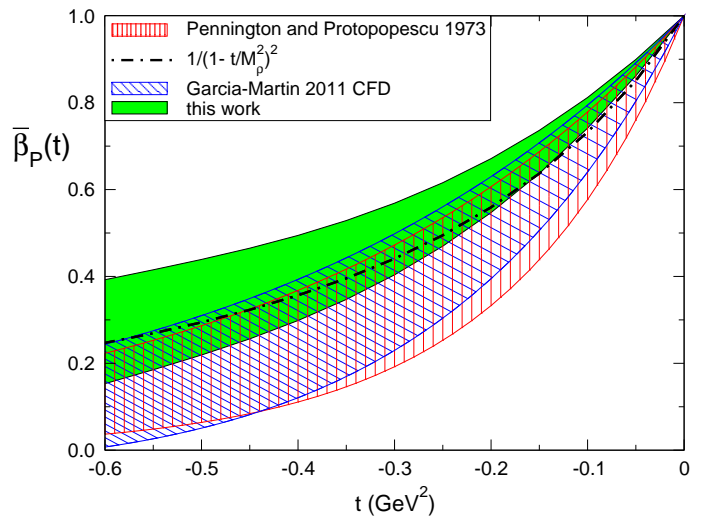


Fig. 7. Profile of the Pomeron residue.

much less rapidly with  $|t|$  than the square of the e.m. form factor.

Results for the structure of the diffraction peak in elastic  $\pi\pi$  scattering would be of considerable interest, in particular in view of possible direct pion-pion collisions at high energies in the near future (for a recent discussion of these prospects see [74]). The TOTEM experiment at the LHC [92], which reaches down to very small momentum transfer in elastic  $NN$  scattering, renewed theoretical interest in topics like the ratio of the real to the imaginary part of the forward scattering amplitude, the comparison of the total elastic and inelastic cross sections, the picture that represents hadrons as black disks, etc. [74, 93, 94]. However, for the reasons given in section 4.1, these questions are beyond the reach of our framework.

## 11.3 Profile of the $\rho$ residue

For the profile of the  $\rho$ , the outcome of our analysis is well described by the numerical representation  $\bar{\beta}_\rho(t) \pm \delta\bar{\beta}_\rho(t)$ , with

$$\begin{aligned} \bar{\beta}_\rho(t) &= 1 + 3.00t + 1.37t^2, \\ \delta\bar{\beta}_\rho(t) &= -0.44t + 0.21t^2. \end{aligned} \quad (58)$$

In this case, the value of the slope is given by

$$b_\rho = 3.4 \pm 0.5 \text{ GeV}^{-2}. \quad (59)$$

Our result for this profile is indicated by the green band in Fig. 8. The residue has a zero at  $t = -0.42^{+0.09}_{-0.24} \text{ GeV}^2$ . The uncertainty band partly overlaps with the one describing the  $f$  residue, which is shown in Fig. 6. Despite the different origin of the two zeros emphasized at the end of section 11.1, the two profiles are consistent with exchange degeneracy.

The recent Regge analysis of  $pp$  and  $\pi p$  data in [71] leads to a rather different picture for the  $t$ -dependence of



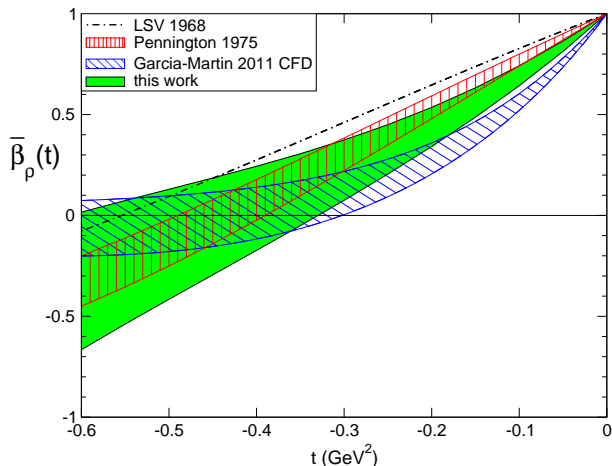


Fig. 8. Profile of the  $\rho$  residue,

the residues. The authors assume factorization, but neglect the difference between the spin-flip and non-flip amplitudes and do not consider data on the charge exchange process. Their representation for  $\beta_\rho(t)$  contains a zero at  $t = -0.153 \pm 0.003 \text{ GeV}^2$  or at  $t = -0.148 \pm 0.003 \text{ GeV}^2$ , depending on whether or not a hard Pomeron component is included. We recall that a zero at small momentum transfer was assumed also in other works, in order to account for the so-called cross-over phenomenon, *i.e.* the equality of the  $\pi^+p$  and  $\pi^-p$  differential cross sections around  $t \sim -0.2 \text{ GeV}^2$ . The Regge representation of [32], for instance, contains a zero at  $t = -0.22 \pm 0.02 \text{ GeV}^2$ . The analysis of the  $\rho$ -dominated charge-exchange process  $\pi^-p \rightarrow \pi^0n$  in [66], however, does not confirm the presence of such a zero. It appears that the cross-over can naturally be explained in the framework of a Regge model with strong absorption for  $\pi N$  scattering [21, 51], without the  $\rho\pi\pi$  residue passing through zero there. At any rate, our results are not consistent with the presence of a zero in  $\beta_\rho(t)$  in the vicinity of the cross-over point.

Fig. 8 contains three other results for the  $\rho$  profile. The one obtained with the LSV model [14] is shown as a dash-dotted line. The zero predicted by this model is compatible with our result. A similar zero position, at  $-0.44 \pm 0.05 \text{ GeV}^2$ , was found in the analysis of Pennington [21], which was also based on the Roy equations and a set of sum rules (the resulting representation for  $\beta_\rho(t)$  was used as an input in [2]). The figure shows that the corresponding band is in very good agreement with the outcome of the present analysis. The figure also shows the most recent version of the  $\rho$ -profile used by the Madrid-Krakow collaboration [37]. Despite some qualitative differences (it is steeper close to the origin and has a larger curvature), their result is in fair agreement with ours.

The uncertainties in  $\bar{\beta}_\rho(t)$  rapidly grow with  $|t|$ : note however that what counts in the applications is not  $\bar{\beta}_\rho(t)$ , but the imaginary part of the amplitude which is proportional to  $\bar{\beta}_\rho(t)(s/s_1)^{\alpha_\rho(t)}$ . At an energy of 2 GeV, the term  $(s/s_1)^{\alpha_\rho(t)}$  drops roughly by a factor of 2 as  $t$  runs from

the upper to the lower end of the interval relevant for the partial wave projections,  $0 \geq t \gtrsim -0.6 \text{ GeV}^2$ .

#### 11.4 Effective residue in the channel with $I_t = 2$

Within errors, the effective residue in the exotic channel,  $\beta_e(t)$ , vanishes at  $t = 0$ . The corresponding profile  $\bar{\beta}_e(t)$  does therefore not represent a meaningful quantity. Instead, Fig. 9 shows the  $t$ -dependence of the residue itself. The upper and lower edges of the band shown can be represented as  $\beta_e(t) \pm \delta\beta_e(t)$ , with

$$\begin{aligned} \beta_e(t) &= -24 - 139t - 94t^2, \\ \delta\beta_e(t) &= 29 - 2t - 19t^2, \end{aligned} \quad (60)$$

and for the slope at  $t = 0$ , we find

$$\beta'_e(0) = -120 \pm 40 \text{ GeV}^{-2}. \quad (61)$$

In the entire range considered here, this residue is small.

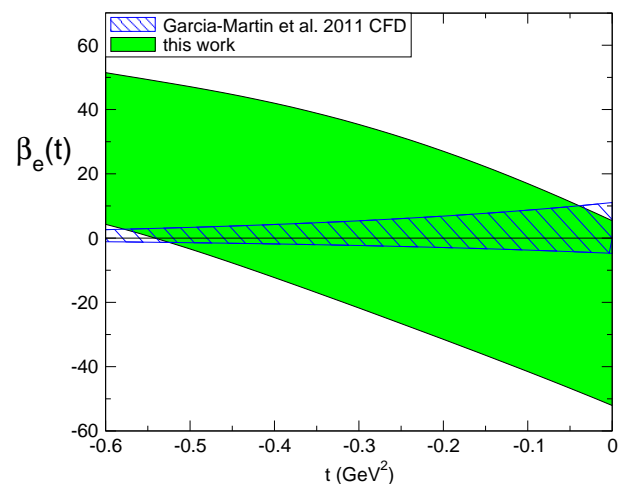


Fig. 9.  $t$ -dependence of the effective residue with  $I_t = 2$

The uncertainty is approximately independent of  $t$ . The value at  $t = 0$  is related to the size of the total cross section in the channel with  $I_t = 2$ , which is shown in Fig. 4c. At 2 GeV, this cross section amounts to  $\sigma^{(2)}(s) = -2 \pm 3 \text{ mb}$ , small compared to the leading term from the Pomeron. At negative values of  $t$ , the residue passes through zero and then becomes positive. In view of the fact that the amplitude is proportional to  $\beta_e(t) s^{\alpha_e(t)}$ , the uncertainty even decreases a little towards the lower end of the range of  $t$ -values where our analysis applies.

Fig. 9 also shows the residue used in the analysis of [36, 37], where the  $t$ -dependence of the residues is taken from [22, 47]. In the latter references, the Regge parameters for  $\pi\pi$  scattering are determined on the basis of factorization. There is, however, barely any direct information on the component of the Regge representation with  $I_t = 2$ . For what concerns  $\beta_e(t)$ , the expectation expressed

in [36, 37] that their Regge parametrization describes experimental data in the region  $1.42 \text{ GeV} \leq \sqrt{s} \leq 20 \text{ GeV}$ ,  $-0.4 \text{ GeV} \leq t \leq 4M_\pi^2$  merely represents an educated guess. Our quantitative analysis does confirm that  $\beta_e(t)$  is small, but it does not support the uncertainties attached to their parametrization, which in our opinion are grossly underestimated.

## 12 Consistency checks

The present section concerns the internal consistency of our results: we compare the contributions to the sum rule and duality relations arising from the low energy region, where we are using the partial wave representation, with those from high energies, for which we use the Regge representation. For the relations to be approximately satisfied, the two contributions must approximately cancel.

### 12.1 Checking the Olsson sum rule

Consider first the Olsson sum rule. The contribution from the integral over the partial waves and from the subtraction constants was analyzed in section 10.2, with the result  $\bar{O}_{\text{PW}} = -0.110^{+0.022}_{-0.015}$ . Evaluating the remainder with the Regge representation constructed in the preceding sections, we obtain  $O_{\text{R}} = 0.106^{+0.016}_{-0.018}$ . The two terms thus indeed cancel within errors. This does not come as a surprise, because the Olsson sum rule occurs among the conditions imposed when constructing the Regge representation. What the agreement mainly checks is that the Olsson sum rule did receive enough weight among the many constraints considered, so that the outcome for the Regge representation does respect it.

### 12.2 Verifying the sum rule $S(t) = 0$

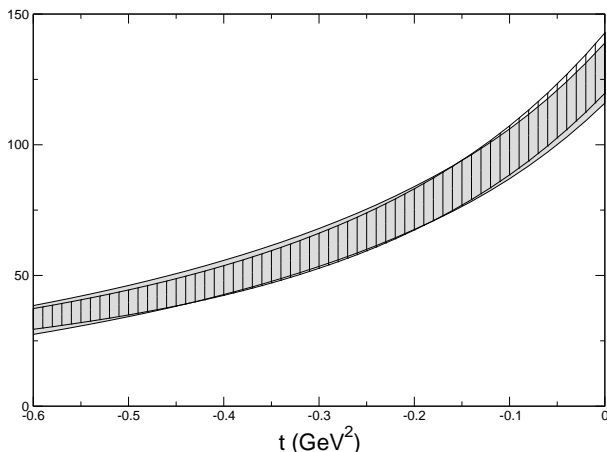


Fig. 10. Validity of the sum rule  $S(t) = 0$ .

In Fig. 10, the low energy contributions to the function  $S(t)$  defined in (39) are shown as a grey band (numerical values in GeV units). To check whether the high energy contributions do approximately cancel these, we flip their sign, so that instead of canceling, the two contributions would become equal if the sum rule was obeyed exactly. The result is indicated by a hatched band. Evidently, the sum rule is very well obeyed within errors.

### 12.3 Checking crossing symmetry

As discussed in section 8, the fact that the crossed channels of elastic  $\pi\pi$  scattering are identical imposes strong constraints on the scattering amplitude. In particular, these imply a set of sum rules of the form  $C_k(t) = 0$ , where  $k = 0, 1, 2$  and  $t$  is a free parameter (see appendix C). In Fig. 11, the red and blue bands for  $C_0(t)$  and  $C_1(t)$  show the partial wave contributions to the integrals occurring in the definition (75) of these functions, while the hatched ones indicate the corresponding Regge contributions, changed in sign (numerical values in GeV units). In order to disentangle the bands for  $C_1(t)$  and  $C_2(t)$ , the sign of the low energy contributions to  $C_2(t)$  is flipped instead of the one from the Regge region. The fact that the partial wave and Regge bands are consistent with one another demonstrates that the sum rules  $C_k(t) = 0$  are well obeyed within errors.

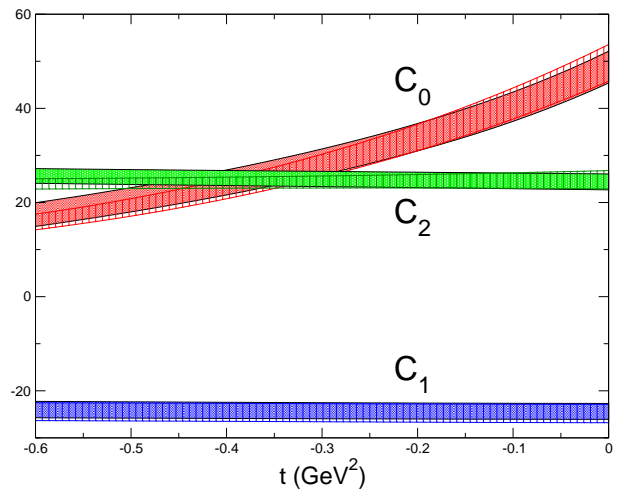


Fig. 11. Validity of the crossing symmetry sum rules.

### 12.4 Checking duality

In the construction of our Regge representation, we made use of a semi-local form of duality: we required the average over the interval  $1.5 \text{ GeV} \leq \sqrt{s} \leq 1.9 \text{ GeV}$  of the partial wave representation for the total cross sections to agree with the average of the Regge representation over the same interval. Moreover, we imposed the same condition also at

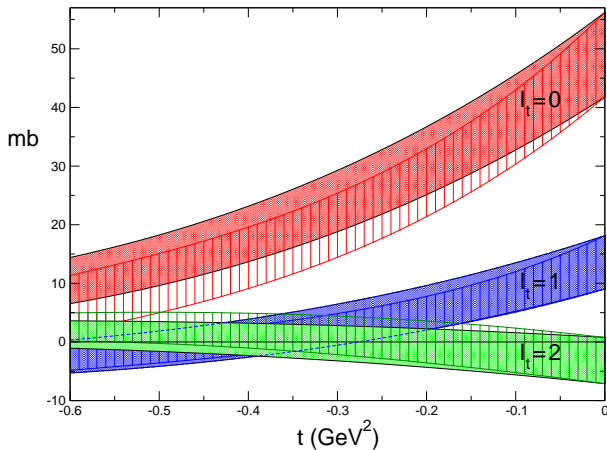


Fig. 12. Duality.

nonzero values of  $t$ , replacing the cross sections by the quantities  $\rho(s)\text{Im}T^{(I_t)}(s, t)$ . In Fig. 12, the full bands indicate the averages over the partial wave representations for these quantities, while the hatched bands represent the averages over the Regge representations (numerical values in mb). The figure shows that the two averages agree: our partial wave and Regge representations do satisfy the semi-local form of duality invoked in the present paper. In fact, since we required the duality conditions for the total cross sections to be strictly obeyed, the full and hatched bands strictly agree at  $t = 0$ .

### 13 Summary and conclusions

In the present paper we have analyzed the high-energy  $\pi\pi$  scattering amplitude. Our main motivation is not high energy *per se* but rather that this part of the amplitude plays a role in the Roy equations, even when these are used to determine the amplitude at low energy. Close to threshold the relevance of high energy is rather limited, but as one moves up, towards 1 GeV and higher, a precise determination of the high-energy contribution becomes important.

We have adopted a Regge parametrization to describe the  $\pi\pi$  scattering amplitude at high energy. Some of its parameters are well known like, *e.g.* the Regge trajectories. Moreover, some Regge residues can be determined from high-energy  $\pi N$  and  $NN$  scattering data [61–63, 71] assuming factorization. Several other parameters, however, are poorly or not at all determined. Aim of the present paper was to pin these down. In order to do this we have worked under the assumption that the partial wave and Regge representations can be joined smoothly in the region between 1.7 and 2 GeV – not only at  $t = 0$  but also as a function of  $t$ , down to about  $-0.6 \text{ GeV}^2$ . In this setting we have imposed a set of sum rules which follow from general principles, like crossing symmetry.

While 2 GeV can hardly be considered asymptotic, it has been already observed in the literature (see [61] and references therein) that, at least on average, duality between the partial wave and Regge representations works

well even at energies that low. In order to both partly test this assumption and make our results less dependent on it, we have supplemented the standard Regge parametrization with pre-asymptotic terms (terms that are suppressed at asymptotic energies with respect to the dominating Regge contributions) and have determined them by requiring that a smooth transition between the partial wave and Regge representations does take place.

For the partial wave representation, we use a simple parametrization which approximately describes the data between 1.15 and 2 GeV. Below 1.15 GeV, we solve the Roy equations – in this region, the exact form of the parametrization becomes irrelevant. In order to solve the Roy equations, we need an input for the high-energy part, which, on the other hand, is what we aim to determine. In summary, we have simultaneously solved a number of constraints – Roy equations, duality and sum rules – which impose relations among the different partial waves at low energy and the high-energy amplitude. This is not an easy task, and to perform it in a way which is as practical as possible we have adopted an iterative scheme:

1. take an input for the Regge parameters;
2. solve the Roy equations for all partial waves up to and including the  $G$  waves;
3. impose the duality and crossing symmetry constraints in order to determine the Regge parameters;
4. if the change in the Regge parameters is significant, go back to 1.

The outcome of this analysis is an improved Regge parametrization of the  $\pi\pi$  scattering amplitude at high energy, which:

1. is consistent with the high-energy data on hadron-hadron scattering under the factorization hypothesis;
2. satisfies the Olsson sum rule and its extension to  $t \neq 0$ , as well as a set of other sum rules which follow from crossing symmetry;
3. smoothly joins the partial wave representation in the region just below 2 GeV, also as far as the  $t$  dependence is concerned.

A summary of the results of the present analysis and of the parameters taken as input is presented in Table 2. Besides the constants  $\beta_\rho(0), p_1, r_1, \beta_e(0)$ , which are relevant for the total cross sections, our analysis also provides the  $t$ -dependence of the residues, which we parametrize in terms of quadratic polynomials. We do not repeat the explicit results for the profiles  $\bar{\beta}_X(t) \equiv \beta_X(t)/\beta_X(0)$  here. They can be found in the equations listed in the table. We stress that our method for determining the  $t$ -dependence of the residues is new and puts their representation on a more solid basis.

The main novelty of our analysis is twofold: First, the introduction of pre-asymptotic terms, which we have shown to be needed in order to reach a smooth transition between the Regge and partial wave representations, especially in the channel with  $I_t = 0$ . Second, the determination of the  $\rho$  residue via the Olsson sum rule, which is much more robust than factorization. These two elements

explain some of the differences found with earlier analyses. For a detailed comparison of our results for the total cross sections, both with data and the literature, we refer the reader to section 10.5.

As we have discussed in section 11.2, the outcome of our calculation for the Pomeron profile is consistent with some of the results available in the literature, but differs from others. Within the accuracy of our calculation, this profile is well described by the square of the pion electromagnetic form factor.

Our results for  $\bar{\beta}_\rho(t)$  indicate that this profile has a zero in the range  $t = -0.42^{+0.09}_{-0.24} \text{ GeV}^2$ . This confirms the results of Pennington [21], which in fact were based on a similar approach. On the other hand, as discussed in section 11.3, the outcome of our calculation is not consistent with parametrizations that explain the cross-over in  $\pi N$  scattering in terms of a zero in  $\bar{\beta}_\rho(t)$ .

As shown in section 11.4, the sum rules studied in the present paper also provide a good handle on the  $t$ -dependence of the Regge amplitude with  $I_t = 2$ . The main result here is that, on the interval  $0 \geq t \gtrsim -0.6 \text{ GeV}^2$ , this amplitude is small compared to the contribution from the Pomeron. The size is comparable to the pre-asymptotic terms in the non-exotic channels with  $I_t = 0, 1$ . As is the case with these, the absolute size of the amplitude with  $I_t = 2$  is subject to large uncertainties.

New solutions of the Roy equations for the  $S, P, D, F$  and  $G$  waves based on this high-energy input have been de-

rived and will be presented in a forthcoming publication. These solutions extend up to 1.15 GeV and are suitable to be used in dispersive analyses of other quantities and processes, like the hadronic vacuum polarization contribution to  $(g-2)_\mu$ ,  $\eta \rightarrow 3\pi$ , Kaon decays in multipion final states etc.

These extended Roy solutions also provide an improved basis for the determination of the pole positions of resonances decaying into two pions, like the  $\sigma$  or the  $\rho$ . We emphasize that extrapolations based on explicit parametrizations of the energy dependence, such as those in [95] or in [96], cannot compete with the analytic continuation provided by dispersion theory. In the case of resonances with a large width, the result for the pole position is subject to large theoretical uncertainties associated with the choice of the parametrization, even if those on the real axis are small [97]. The result for the mass and width of the  $\sigma$  obtained by extrapolating the explicit parametrization in [95], for instance, differs significantly from the pole position calculated on the basis of the Roy equations [3], despite the excellent agreement on the real axis. The dispersive method has the advantage that it provides a complete error analysis which includes, in particular, also the uncertainties associated with the presence of inelastic channels. The calculations performed in [98, 99] corroborate this statement: the result for the pole position agrees with [3], within the quoted errors.

Parameter	Value	Source
$\alpha_P(0)$	1	PDG 2011
$\alpha_f(0)$	$0.54 \pm 0.05$	our estimate
$\alpha_\rho(0)$	$0.45 \pm 0.02$	our estimate
$\alpha_e(0)$	0	our estimate
$\alpha'_P(0)$	$0.25 \pm 0.05 \text{ GeV}^{-2}$	diffraction peak
$\alpha'_f(0)$	$0.90 \pm 0.05 \text{ GeV}^{-2}$	Chew-Frautschi plot
$\alpha'_\rho(0)$	$0.91 \pm 0.02 \text{ GeV}^{-2}$	Chew-Frautschi plot
$\alpha'_e(0)$	$0.5 \pm 0.1 \text{ GeV}^{-2}$	our estimate
$\bar{B}$	$0.025 \pm 0.001$	PDG 2011
$\sqrt{s_0}$	$5.38 \pm 0.50 \text{ GeV}$	PDG 2011
$\beta_P(0)$	$94 \pm 1$	factorization
$\beta_f(0)$	$69 \pm 2$	factorization
$\bar{\beta}_f(t)$	equation (52)	linearity, no ghosts
$\beta_\rho(0)$	$84^{+13}_{-16}$	Olsson s.r., duality
$\beta_e(0)$	$-24 \pm 29$	duality
$p_1$	$-0.8 \pm 0.6$	duality
$r_1$	$-0.8^{+0.8}_{-0.7}$	Olsson s.r., duality
$b_P$	$2.5 \pm 0.4 \text{ GeV}^{-2}$	sum rules, duality
$b_\rho$	$3.4 \pm 0.5 \text{ GeV}^{-2}$	sum rules, duality
$\beta'_e(0)$	$-120 \pm 40 \text{ GeV}^{-2}$	sum rules, duality
$\bar{\beta}_P(t)$	equation (55)	sum rules, duality
$\bar{\beta}_\rho(t)$	equation (58)	sum rules, duality
$\beta_e(t)$	equation (60)	sum rules, duality

**Table 2.** Regge representation of the scattering amplitude. The upper part lists the range used for the input parameters, while the lower part indicates the results of our calculation.

**Acknowledgments:** IC acknowledges support from CNCS, Contract Idei Nr.464/2009. The Albert Einstein Center for Fundamental Physics at the University of Bern is supported by the “Innovations- und Kooperationsprojekt C-13” of the “Schweizerische Universitätskonferenz SUK/CRUS”. This work was partially supported by the Swiss National Science Foundation and by EU contract MRTN-CT-2006-035482 (Flavianet).

## A Literature on the Regge parameters

Most of the literature on the Regge parameters deals with  $NN$  and  $\pi N$  scattering, for which fits of various experimental data sets were performed. The parameters relevant for  $\pi\pi$  scattering are in general obtained only indirectly, using factorization [47, 65, 71, 74]. Several modifications of the standard expression (1) were also considered in the literature: for instance, an additional factor  $\Gamma(\alpha(t))$  is often introduced in the denominator of (1) in order to remove the unphysical poles due to  $\sin \pi\alpha$ . Other factors dependent on the trajectory, which remove unphysical poles, are adopted in [47], [32, 34–37], [66, 75], etc.

In the present review, we mainly consider the trajectory parameters, the residues at  $t = 0$  and the slope of the Pomeron profile at this point. For simplicity, we mostly quote only the central values, omitting the errors. We mention that, although the values reported in the literature for a certain parameter may be quite different, correla-

tions with different values of other parameters may lead to a similar overall description.

### A.1 Pomeron

In the early literature, the contribution of the Pomeron to the total cross sections was assumed to be energy independent, which in view of (8) corresponds to a trajectory with intercept  $\alpha_P(0) = 1$ . In equation (5), the Pomeron is described by a triple Regge pole with  $\alpha_P(0) = 1$ , leading to a cross section that contains a constant term and a term which grows with  $\ln^2 s$ . The ‘‘soft Pomeron’’ [55] with an intercept slightly larger than 1 (for instance,  $\alpha_P(0) = 1.093$  [58] or  $\alpha_P(0) = 1.08$  [61]), also yields a very good description over a very wide range of energies, while a ‘‘hard’’ Pomeron with  $\alpha_P(0) = 1.45$  was shown [57] to explain the data on  $ep$  scattering at HERA. In [71] both of these variants of the Pomeron are used for the description of  $pp$ ,  $\pi p$  and  $Kp$  elastic scattering at small  $t$ .

Information on the  $t$ -dependence of the trajectory is obtained from the slope of the diffraction peak in  $pp$  and  $\pi p$  collisions at high energies:

$$B_{ap}(s) = \partial_t \ln [d\sigma^{ap}(s, t)/dt]_{t \rightarrow 0}, \quad (62)$$

where  $a$  stands for  $p, \bar{p}$  or  $\pi^\pm$ . The quantity (62) is expressed as

$$B_{ap}(s) = 2[b_P^{ap} + \alpha'_P(0) \ln(s/s_1)], \quad (63)$$

in terms of the slope of the trajectory,  $\alpha'_P(0)$ , and the slope  $b_P^{ap}$  of the Pomeron profile at  $t = 0$ , defined in the case of  $\pi\pi$  scattering in equation (53).

The slope of the diffraction peak in proton-proton scattering was measured by many experiments at various energies (for references on the data sets see [71, 72]). Recently, the slope  $B_{pp}$  was measured at  $\sqrt{s} = 7$  TeV by the TOTEM Collaboration at LHC [92]. The trajectory slope  $\alpha'_P(0) = 0.25$  was shown to be consistent with high energy data, in particular in the context of the soft Pomeron [54]. A recent comprehensive analysis [72], based on the available experimental data on  $pp$  and  $\bar{p}p$  scattering over a large energy scale, reports the average value  $\alpha'_P(0) = 0.24$ .

Recent choices of the Pomeron trajectory are:

$\alpha_P(t) = 1.0 + 0.20t$  [37],  $1.09 + 0.33t$  [71],  $1.08 + 0.25t$  [75], to be compared with the input used in the present paper,  $\alpha_P(t) = 1 + (0.25 \pm 0.05)t$ .

The Pomeron residue  $\beta_P(t) \equiv \beta_P^{\pi\pi}(t)$  is known with less precision. For the value at  $t = 0$ , we quote:  $\beta_P(0) = 46$  [2], 118 [32], 99 [37], 66 [65], 98 [74], to be compared with the input we are using,  $\beta_P(0) = 94 \pm 1$ . Fig. 4a. illustrates the fact that the value used in [2] is on the low side, while the one in [74] is high. The value derived in [65] (which is based on factorization and the older parametrization of  $NN$  and  $\pi N$  data given in [55]) is also low, but this is partly compensated by a higher value for  $\beta_f(0)$ .

As concerns the  $t$ -dependence near  $t = 0$ , an exponential form

$$\beta_P^{ab}(t) = \beta_P^{ab}(0)e^{b_P^{ab}t}, \quad (64)$$

was often assumed for various types of elastic reactions  $ab \rightarrow ab$  (early references are [45, 47, 50], for more recent work see for instance [32, 34–37], [66, 75]). For the slope in  $\pi\pi$  scattering,  $b_P \equiv b_P^{\pi\pi}$ , factorization implies

$$b_P = 2b_P^{\pi p} - b_P^{pp}. \quad (65)$$

Since the  $\pi p$  data at  $t \neq 0$  are less accurate, the extraction of  $b_P$  from this relation is not very precise. The values proposed in the literature scatter wildly:  $b_P = 4$  [19], 3.3 [37], 0.42 [47], 0.79 [71], to be compared with the result of our calculation,  $b_P = 2.5 \pm 0.4$ .

### A.2 $f$ pole

The parametrization of the  $f$  Regge pole (denoted also as  $P'$  in the literature [32, 34–37, 47]) is linked with the one of the Pomeron. Indeed, both contribute to the amplitude with  $I_t = 0$  and are largely indiscernible. The relative weight of the contributions from Pomeron and  $f$  depends on the parametrization chosen for the Pomeron. For one of the fits obtained by Rarita et al. [47], for instance, the Pomeron dominates over the  $f$  already below 1.8 GeV, while for the others this is the case only at much higher energies.

Recent parametrizations of the  $f$ -trajectory are:

$\alpha_f(t) = 0.53 + 0.90t$  [37],  $0.69 + 0.80t$  [59],  $0.96 + 0.58t + 0.03t^2$  [59],  $0.61 + 0.82t$  [71],  $0.71 + 0.83t$  [75], while we are using  $\alpha_f(t) = (0.54 \pm 0.05) + (0.90 \pm 0.05)t$  as an input.

The values of  $\beta_f(0)$  proposed in the earlier literature [21, 47] cover a large range. Some values adopted recently are (compare section 10.5):  $\beta_f(0) = 108$  [2], 32 [37], 103 [65], 153 [71], 123 [74], to be compared with the input we are relying on,  $\beta_f(0) = 69 \pm 2$ .

### A.3 $\rho$ pole

The  $\rho$  trajectory is relatively well known. Some choices made in the literature are:

$\alpha_\rho(t) = 0.53 + 0.90t - 0.15t^2$  [37],  $0.44 + 0.96t - 0.02t^2$  [59],  $0.48 + 0.88t$  [59],  $0.53 + 0.8t$  [66, 75],  $0.47 + 0.91t$  [71], while our estimate reads  $\alpha_\rho(t) = (0.45 \pm 0.02) + (0.91 \pm 0.02)t$ .

For the residue, the values  $\beta_\rho(0) \approx 104.2$  given by Kane and Seidl [51],  $\beta_\rho(0) \approx 107.6$  of Irving and Worden [52] and  $\beta_\rho(0) \approx 116$  predicted by the Lovelace-Shapiro-Veneziano model [14] are on the high side. Pennington [21] obtains  $\beta_\rho(0) \approx 72$ , a value which was adopted also in [2]. These numbers are to be compared with the outcome of our calculation, which reads  $\beta_\rho(0) = 84_{-16}^{+13}$ .

A smaller value,  $\beta_\rho(0) = 33.2$  was proposed in [32], invoking consistency with data on  $\pi\pi$  scattering at high energies. In the subsequent papers [34–37], the authors resorted to dispersive analyses of the pion-pion amplitude and gradually increased their estimate:  $\beta_\rho(0) = 37.1$  [34], 48.2 [36], 58.4 [37]—CFD solution. The difference between the values obtained in [34]–[36] and our result is due partly

to a different shape of the isoscalar  $S$  wave below 1 GeV (the phase shift  $\delta_0^0(s)$  given in these works displays an unphysical ‘‘hump’’ around 0.8 GeV, see the discussion in [97, 100]). We mention that in the most recent result of this group, quoted as CFD solution in [37], this hump is no longer present.

Other recent values are  $\beta_\rho(0) = 84$  (obtained in [65] with factorization, using the older parametrization of cross sections in [55]), which is consistent with our result, and the very small value  $\beta_\rho(0) = 9.8$  found in [74], which is discussed in section 10.5.

The results given in the literature for the residue  $\beta_\rho(t)$  at  $t \neq 0$  are rather controversial. The values obtained from dispersion sum rules for the  $\pi\pi$  amplitude in the seventies [17, 18, 21] were not conclusive, due to the poor quality of the data at low energies. The phenomenological information provided by factorization was also rather poor: since the contribution of the  $\rho$ -pole to the forward  $NN$  amplitudes is small, it was neglected altogether in some of the early fits [47]. The studies of the  $\rho$ -dominated charge exchange process  $\pi^- p \rightarrow \pi^0 n$  indicated that indeed the spin-flip  $\rho NN$  coupling is larger than the non-flip coupling, which is the only one contributing to the forward  $NN$  scattering amplitude. This feature is confirmed by the recent analysis of the pion-nucleon charge exchange amplitudes [66].

#### A.4 Regge cuts

The Regge cuts are introduced in phenomenological analyses especially for extending the validity of the Regge model to larger values of  $|t|$  (see for instance the recent works [65, 66]). As we are interested in a rather small range of  $t$ , we consider a Regge cut only for the description of the exotic amplitude with  $I_t = 2$ , where it is the dominant contribution.

The information about this term is poor, since it does not contribute above 5 GeV, where the Regge fits to the  $NN$  and  $\pi N$  amplitudes are usually done [63, 71, 73, 74]. Alternative treatments based on sum rules for  $\pi\pi$  scattering in the seventies were not conclusive. Pennington [21] notices a great sensitivity of the finite-energy sum rule for the amplitude with  $I_t = 2$  with respect to the transition point from low to high energy regimes. He assumes  $\beta_e(0) \approx 0$ , this value being adopted also in [2]. A small effective residue  $\beta_e(t)$  appearing in equation (27) can occur from cancellations of the  $\rho - \rho$  and  $a_2 - a_2$  cuts, as argued by Worden [48], using symmetry arguments in the Reggeon-calculus of Gribov [49]. In [37] the authors obtain  $\beta_e(0) = 8$  in the UFD fit, and  $\beta_e(0) = 3$  in the CFD fit. This is consistent with our result, which comes with a large error:  $\beta_e(0) = -24 \pm 29$ .

The  $t$ -dependence of  $\beta_e(t)$  is also poorly known. In [37], the residue is taken to be proportional  $\exp b_e t$ , with  $b_e = 2.4$ . The ansatz prevents  $\beta_e(t)$  from passing through zero and makes it shrink if the momentum transfer grows (compare Fig. 9). The numerical value for the slope is  $\beta_e'(0) = 20$  and  $\beta_e'(0) = 8$  for the UFD and CFD fits, respectively. Our framework does not support this ansatz:

the sum rules require a zero and a comparatively large, negative slope,  $\beta_e'(0) = -120(40)$ .

## B Roy equations

### B.1 Fixed- $t$ dispersion relation

The derivation of the Roy equations (see [1] and appendix A of [2]) is based on the fixed- $t$  dispersion relation obeyed by the  $s$ -channel isospin amplitudes  $\mathbf{T} = (T^0, T^1, T^2)$  in the interval  $-28M_\pi^2 < t < 4M_\pi^2$ , written as [1]

$$\begin{aligned} \mathbf{T}(s, t) &= (4M_\pi^2)^{-1} (s \mathbf{1} + t C_{st} + u C_{su}) \mathbf{T}(4M_\pi^2, 0) \\ &+ \int_{4M_\pi^2}^{\infty} ds' g_2(s, t, s') \text{Im} \mathbf{T}(s', 0) \\ &+ \int_{4M_\pi^2}^{\infty} ds' g_3(s, t, s') \text{Im} \mathbf{T}(s', t). \end{aligned} \quad (66)$$

The subtraction term is fixed by the  $S$ -wave scattering lengths:

$$\mathbf{T}(4M_\pi^2, 0) = 32 \pi (a_0^0, 0, a_0^2), \quad (67)$$

the crossing matrices  $C_{tu} = C_{ut}$ ,  $C_{su} = C_{us}$ ,  $C_{st} = C_{ts}$  are given by

$$\begin{aligned} C_{tu} &= \begin{pmatrix} 1 & 0 & 0 \\ 0 & -1 & 0 \\ 0 & 0 & 1 \end{pmatrix} & C_{su} &= \begin{pmatrix} \frac{1}{3} & -1 & \frac{5}{6} \\ -\frac{1}{3} & \frac{1}{2} & \frac{5}{6} \\ \frac{1}{3} & \frac{1}{2} & \frac{1}{6} \end{pmatrix} \\ C_{st} &= \begin{pmatrix} \frac{1}{3} & 1 & \frac{5}{6} \\ \frac{1}{3} & \frac{1}{2} & -\frac{5}{6} \\ \frac{1}{3} & -\frac{1}{2} & \frac{1}{6} \end{pmatrix} \end{aligned}$$

and the kernels  $g_2(s, t, s')$ ,  $g_3(s, t, s')$  represent  $3 \times 3$  matrices built with  $C_{st}$ ,  $C_{tu}$  and  $C_{su}$ ,

$$\begin{aligned} g_2(s, t, s') &= -\frac{t}{\pi s' (s' - 4M_\pi^2)} (u C_{st} + s C_{st} C_{tu}) \times \\ &\quad \left( \frac{\mathbf{1}}{s' - t} + \frac{C_{su}}{s' - u_0} \right), \\ g_3(s, t, s') &= -\frac{s u}{\pi s' (s' - u_0)} \left( \frac{\mathbf{1}}{s' - s} + \frac{C_{su}}{s' - u} \right), \end{aligned} \quad (68)$$

where  $u = 4M_\pi^2 - s - t$  and  $u_0 = 4M_\pi^2 - t$ .

We add a comment concerning the subtractions. As emphasized in [37], a single subtraction suffices: the Olsson sum rule (37) can be used to express one of the two subtraction constants in terms of the other. The resulting set of relations is referred to as the GKPY-equations. Conversely, the dispersive representation for  $\mathbf{T}(s, t)$  obtained in that framework [37] differs from the one in (66) by a multiple of the Olsson sum rule. The advantage of using a single subtraction is that this allows a better determination of  $a_0^0$  and  $a_0^2$  from experiment (see the discussion at the end of section 5). The price to pay is that the dispersive representation for the partial waves then becomes

more sensitive to the high energy part of the input used, because the GKPY-equations converge less rapidly than the Roy equations. As we are relying on the theoretical predictions for  $a_0^0$  and  $a_0^2$ , retreating to a single subtraction is no gain for us.

## B.2 Dispersive representation of the partial waves

Exploiting crossing symmetry, the partial wave projection of the amplitude in (31) can be written in a form that involves a smaller range of  $t$ -values:

$$t_\ell^I(s) = \frac{1}{32\pi} \int_0^1 dz P_\ell(z) T^I(s, t_z). \quad (69)$$

This step extends the range of validity of Roy's representation [1],

$$t_\ell^I(s) = k_\ell^I(s) + \sum_{I'=0}^2 \sum_{\ell'=0}^{\infty} \int_{4M_\pi^2}^{\infty} ds' K_{\ell\ell'}^{II'}(s, s') \text{Im } t_{\ell'}^{I'}(s'). \quad (70)$$

The term  $k_\ell^I(s)$  denotes the partial wave projection of the subtraction term, which shows up only in the  $S$ - and  $P$ -waves,

$$k_\ell^I(s) = a_0^I \delta_\ell^0 + \frac{s - 4M_\pi^2}{4M_\pi^2} (2a_0^0 - 5a_0^2) \times \left( \frac{1}{3} \delta_0^I \delta_\ell^0 + \frac{1}{18} \delta_1^I \delta_\ell^1 - \frac{1}{6} \delta_2^I \delta_\ell^0 \right). \quad (71)$$

The kernels  $K_{\ell\ell'}^{II'}(s, s')$  are explicitly known functions (see appendix A of [2]). They contain a diagonal, singular Cauchy kernel that generates the right hand cut in the partial wave amplitudes, as well as a logarithmically singular piece that accounts for the left hand cut. The validity of these equations has rigorously been established on the interval  $-4M_\pi^2 < s < 68M_\pi^2 = (1.15 \text{ GeV})^2$ .

In [2], Roy's equations were solved for the  $S$ - and  $P$ -waves in the region  $\sqrt{s} \leq 0.8 \text{ GeV}$ . In the present paper we solve these equations in the whole range  $\sqrt{s} \leq 1.15 \text{ GeV}$ , including also the higher partial waves, which become increasingly important as the energy grows, because they are given more weight in the sum and the angular momentum barrier becomes less effective: for instance, above 1.6 GeV, the  $S$ -wave accounts for less than a quarter of the total cross section with  $I_s = 0$ . In order to have a reliable description, we solved the Roy equations for the waves with  $\ell \leq 4$  below 1.15 GeV and made use of the fact that, below 2 GeV, the masses, widths and  $\pi\pi$  branching fractions of the resonances are now known quite well [64]. A detailed description of the solution of the Roy equations will be given elsewhere [38] – in the following, we limit ourselves to a cursory discussion.

## B.3 Input used when solving the Roy equations

The input required for the construction of the solutions of the Roy equations was outlined in section 5. There, we also

reviewed the status of our knowledge of the subtraction constants. In the present appendix, we briefly discuss the other elements of the input used for the partial waves.

### B.3.1 Phases

Our analysis relies on the following phenomenological estimates for values of the  $S$ - and  $P$ -wave phase shifts in the low energy region ( $\sqrt{s_A} = 0.8 \text{ GeV}$ ,  $\sqrt{s_{max}} = 1.15 \text{ GeV}$ ):

$$\begin{aligned} \delta_0^0(s_A) &= 82.3_{-4}^{+10}, & (72) \\ \delta_0^0(4M_K^2) &= 185^\circ \pm 10^\circ, \\ \delta_0^0(s_{max}) &= 260^\circ \pm 10^\circ, \\ \delta_1^1(s_A) &= 108.9^\circ \pm 2^\circ, \\ \delta_1^1(s_{max}) &= 166.5^\circ \pm 2^\circ. \end{aligned}$$

We briefly comment on these estimates.

The phase shift analyses available at the time were used in [2] to estimate the  $S^0$  phase shift at 0.8 GeV, with the result  $\delta_0^0(s_A) = 82.3^\circ \pm 3.4^\circ$ . This estimate was criticized in [32], however, and significantly higher values were suggested. We did reply to this objection [33], but when analyzing the consequences of the representation for the  $S^0$ -wave for the mass and width of the  $\sigma$  [39], we decided to inflate the uncertainty range by a factor of 2, in order to make it evident that the outcome is not tied to an input which at the time appeared to be controversial.

In the meantime, the dust settled – the discrepancy disappeared: the result  $\delta_0^0(s_A) = 85.7^\circ \pm 1.6^\circ$  obtained in the most recent paper of the Madrid-Krakow collaboration (Table XII in [37]) differs from the old estimate in [2] by less than one standard deviation. Moreover, the thorough analysis of the experimental situation concerning the  $S^0$  phase shift in [95] fully confirms the results of [2,3], also with regard to the value at 0.8 GeV. Last, not least, we point to a recent paper by Moussallam [99], who has analyzed the problem, solving the Roy equations with matching point at  $2M_K$  and relying on the experimental results for the scattering lengths obtained by NA48/2 [83] to fix the subtraction constants. He shows that, currently, the uncertainties in the value of  $\delta_0^0(s_A)$  are dominated by those in the input used for the elasticity above  $K\bar{K}$  threshold: while the shallow dip in  $\eta_0^0(s)$  obtained from the data on the inelastic channels leads to  $\delta_0^0(s_A) = 82.9^\circ \pm 1.7^\circ$ , the deep dip indicated by the data on elastic scattering yields  $\delta_0^0(s_A) = 80.9^\circ \pm 1.4^\circ$ . Both of these results are within the range estimated in [2]. Hence we might just as well return to that estimate, but, for the time being, we prefer to stick to the broad uncertainty range adopted in [39] – we plan to examine the present experimental situation concerning the low partial waves in a forthcoming article [38].

Phase shift analysis indicates that  $\delta_0^0(s)$  passes through  $180^\circ$  in the vicinity of  $K\bar{K}$  threshold, but it is still not known for certain whether this happens below or above that point, although the second option appears to be more likely. The error bar attached to our estimate allows for both possibilities. The values for  $\delta_0^0(4M_K^2)$  given in [99]

are consistent with our estimate in (72), albeit somewhat higher.

The P<sup>1</sup>-wave is experimentally very well determined through the data on the e.m. form factor of the pion, so that our estimates for the phase shifts for  $\delta_1^1(s_A)$  and  $\delta_1^1(s_{max})$  in (72) come with small errors.

The list (72) does not contain entries for the exotic phase shift  $\delta_0^2(s)$ . The reason is the following. As discussed in [2], the solutions of the Roy equations in general develop a cusp at the matching point, which in the present framework is taken at  $\sqrt{s_{max}} = 1.15$  GeV. We remove the unphysical phenomenon by requiring the phase shifts as well as their derivatives to be continuous at the matching point. This in effect imposes a condition on the behaviour of the imaginary parts above this point: we find acceptable solutions only if we do not prescribe the value of  $\delta_0^2(s_{max})$ , but let it float (for a more thorough discussion, see [2]). The same holds for the higher partial waves: the requirement that the phase shift and its derivative are continuous at the matching point admits solutions only if the value of the phase at this point is not prescribed.

For the numerical evaluation of the Roy equations, we need an explicit *parametrization* of the phases. Since the solution is uniquely determined, the choice of the parametrization is a matter of convenience – the only requirement to be met is that it is flexible enough to come close to the exact solution. In the case of the S<sup>0</sup>-wave, the fact that there is a resonance in the immediate vicinity of  $K\bar{K}$  threshold entails a rather intricate behaviour there and special care is needed to find solutions of good quality, but for the other waves, we did not encounter such problems. For details, we refer to [38].

### B.3.2 Elasticities

The input used for the elasticity of the partial waves in the region where the Roy equations are solved plays a significant role, not only in resolving the structure of the S<sup>0</sup> wave in the vicinity of  $K\bar{K}$  threshold, for instance, but also when analyzing the behaviour of the partial waves off the real axis, in order to determine the position of the resonance poles, such as the one of the  $\sigma$ . The elasticities ensure that the effects on the elastic  $\pi\pi$  scattering amplitude generated by inelastic processes like  $\pi\pi \leftrightarrow K\bar{K}$ , for instance, are properly accounted for.

The interference between the  $K\bar{K}$  cut and the pole associated with the  $f_0(980)$  generates a dip in the elasticity of S<sup>0</sup>, immediately above  $\sqrt{s} = 2M_K$ . In the region between  $2M_K$  and 1.15 GeV, where it matters for our analysis, the uncertainties in the elasticity of S<sup>0</sup> are gradually becoming smaller. For a recent, very thorough analysis of this field, we refer to [99]. We describe the behaviour by means of the Flatté formula [101] and vary the parameters contained therein in a rather broad range, so that the uncertainty band for  $\eta_0^0(s)$  generously covers the available parametrizations. The inelasticities of P<sup>1</sup> and S<sup>2</sup> are also estimated on the basis of available phase shift analyses. For the higher partial waves with  $I_s = 0$  or 1, we use

a Breit-Wigner parametrization and calculate the corresponding inelasticities from mass, width and branching fraction for the decay into  $\pi\pi$  quoted in the data tables. The exotic waves D<sup>2</sup> and G<sup>2</sup> are driven by the other partial waves. Since their inelasticities are very small, these barely affect our results. For a more thorough discussion, we refer to [38].

### B.3.3 Imaginary parts

Although phenomenology does reduce the range allowed by unitarity,  $0 \leq \text{Im } t_\ell^I(s) \leq 1/\rho(s)$ , the uncertainties in the behaviour of the partial wave imaginary parts above the matching point are considerable.

We use a crude parametrization involving Breit-Wigner terms for the resonances and polynomials for the background, impose continuity of function and derivative at the matching point and allow for one free parameter in the representation used, for each one of the partial waves with  $\ell \leq 4$ . It is convenient to identify the free parameter with the value of the corresponding imaginary part at  $\sqrt{s_b} = 2$  GeV. Our estimates for the latter read:

$$\begin{aligned} \text{Im } t_0^0(s_b) &= 0.4 \pm 0.25, & \text{Im } t_1^1(s_b) &= 0.26 \pm 0.13, & (73) \\ \text{Im } t_0^2(s_b) &= 0.3 \pm 0.15, & \text{Im } t_2^0(s_b) &= 0.2 \pm 0.075, \\ \text{Im } t_3^1(s_b) &= 0.23 \pm 0.07, & \text{Im } t_2^2(s_b) &= 0.12 \pm 0.06, \\ \text{Im } t_4^0(s_b) &= 0.22 \pm 0.03, & \text{Im } t_4^2(s_b) &= 0.01 \pm 0.01. \end{aligned}$$

We plan to describe the parametrization used in more detail [38].

## C Sum rules from crossing symmetry

A set of sum rules for fixed  $t$  is obtained by taking the first derivative with respect to  $s$  of the l.h.s. of (41) and then setting  $s = 0$ . Since the resulting expression has a zero both at  $t = 0$  and at  $t = 4M_\pi^2$ , it is convenient to divide by the factor  $t(t - 4M_\pi^2)$ . The sum rules then take the form

$$C_k(t) = 0, \quad k = 0, 1, 2, \quad (74)$$

where  $C_0(t)$ ,  $C_1(t)$ ,  $C_2(t)$  are integrals over the imaginary part of the scattering amplitude:

$$\begin{aligned} C_k(t) &\equiv \int_{4M_\pi^2}^{\infty} ds n_k(s, t) \text{Im } \bar{T}^{(k)}(s, t) & (75) \\ &+ \int_{4M_\pi^2}^{\infty} ds f_k(s, t) \text{Im } T^1(s, 0) \\ &+ \sum_{\ell=0}^2 \int_{4M_\pi^2}^{\infty} ds h_{k\ell}(s, t) \partial_{t'} \text{Im } T^\ell(s, t') \Big|_{t' \rightarrow 0}. \end{aligned}$$

The functions  $\text{Im } \bar{T}^{(0)}(s, t)$ ,  $\text{Im } \bar{T}^{(1)}(s, t)$ ,  $\text{Im } \bar{T}^{(2)}(s, t)$  are defined in (40). The first line shows that the sum rules decouple, in the sense that the  $t$ -dependent part of the scattering amplitude enters with definite isospin in the



$t$ -channel. The explicit expressions for the corresponding kernels read

$$\begin{aligned} n_0(s, t) &= \frac{2s + t - 4M_\pi^2}{\pi s^2 (s + t - 4M_\pi^2)^2}, \\ n_1(s, t) &= \frac{t - 4M_\pi^2}{\pi s^2 (s + t - 4M_\pi^2)^2}, \\ n_2(s, t) &= \frac{2s + t - 4M_\pi^2}{\pi s^2 (s + t - 4M_\pi^2)^2}. \end{aligned} \quad (76)$$

The diagonal elements of  $h_{k\ell}(s, t)$  are of the form

$$\begin{aligned} h_{00}(s, t) &= \frac{-4s - 2t + 12M_\pi^2}{3\pi s(s - 4M_\pi^2)(s - t)(s + t - 4M_\pi^2)}, \\ h_{11}(s, t) &= \frac{-3s - t + 8M_\pi^2}{2\pi s(s - 4M_\pi^2)(s - t)(s + t - 4M_\pi^2)}, \\ h_{22}(s, t) &= \frac{-7s - 5t + 24M_\pi^2}{6\pi s(s - 4M_\pi^2)(s - t)(s + t - 4M_\pi^2)}. \end{aligned} \quad (77)$$

The off-diagonal ones are given by

$$\begin{aligned} h_{k\ell}(s, t) &= \frac{c_{k\ell}}{6\pi s(s - 4M_\pi^2)(s + t - 4M_\pi^2)}, \\ c_{01} &= 6, & c_{02} &= -10, \\ c_{10} &= 2, & c_{12} &= -5, \\ c_{20} &= -2, & c_{21} &= -3. \end{aligned} \quad (78)$$

The kernels in the second line of (75) can be expressed in terms of those listed above:

$$\begin{aligned} f_k(s, t) &= -\frac{c_k n_k(s, t) + 2h_{k1}(s, t)}{s - 4M_\pi^2}, \\ c_0 &= 2, & c_1 &= 1, & c_2 &= -1. \end{aligned} \quad (79)$$

As in the case of  $S(t)$ , the integrands in (75) display a fictitious double pole for  $s = 4M_\pi^2 - t$ , but the residue of the singularity vanishes for a crossing symmetric integrand. At  $t = 0$ , the three sum rules (74) reduce to a single one, in fact one that had been made use of already earlier.<sup>10</sup>

Since the contribution from the S- and P-waves is manifestly crossing symmetric, these waves do not show up in the above sum rules. For the S-waves, which generate a  $t$ -independent contribution, that is manifest: these waves drop out, in  $\text{Im}\bar{T}(s, t)$ , in  $\text{Im}T^1(s, 0)$ , as well as in the terms involving the partial derivative with respect to  $t$ . The P<sup>1</sup>-wave, on the other hand does generate a contribution to these quantities – it drops out only in the sum, on account of the relation (79) between the kernels.

## D Details of minimization procedure

In the present appendix, we specify the discrepancy function that enters the procedure used to solve the sum rules and duality conditions, as described in section 9. For a

given input, these amount to constraints imposed on the Regge output variables,

$$v_{out}^R = \{p_1, b_P, c_P, \beta_\rho(0), r_1, b_\rho, c_\rho, \beta_e(0), b_e, c_e\}. \quad (80)$$

We evaluate the  $t$ -dependent conditions on a finite number of points, using the lattice

$$t_n = n t_1, \quad t_1 = -0.1 \text{ GeV}^2, \quad n = 0, \dots, 6. \quad (81)$$

The sum rules and duality conditions then amount to a finite number of relations of the form

$$S_r^{\text{PW}} + S_r^R(v_{out}^R) = 0, \quad r = 1, 2, \dots$$

The part  $S_r^{\text{PW}}$  represents the contribution from the region where we use the partial wave representation, while the remainder is calculated with the Regge parametrization.

The duality conditions for the total cross sections are solved as algebraic constraints for the variables  $p_1, r_1, \beta_e(0)$ . The remaining variables in  $v_{out}^R$  are determined by minimizing the discrepancy function

$$\chi^2(v_{out}^R) = \sum_r \lambda_r [S_r^{\text{PW}} + S_r^R(v_{out}^R)]^2, \quad (82)$$

where the sum extends over all constraints except the duality conditions at  $t = 0$ . The factors  $\lambda_r$  specify the weights of the remaining conditions in the minimization process. We determine these with the response of the term  $S_r^{\text{PW}}$  to variations of the partial wave input: vary the input parameters within the estimated uncertainty range, calculate the responses generated by these variations in  $S_r^{\text{PW}}$ , evaluate the sum  $\Delta_r$  over the squares of these responses and set  $\lambda_r = 1/\Delta_r$ . The choice of the weights is not of crucial importance, because the various sum rules and duality conditions are consistent with one another. The particular choice made homogenizes the set of relations, giving little weight to those constraints that are sensitive to the uncertainties in our partial wave representation and thus contain little information about the Regge output parameters, which we determine by minimizing  $\chi^2(v_{out}^R)$ .

## References

1. S.M. Roy, Phys. Lett. B **36**, 353 (1971).
2. B. Ananthanarayan, G. Colangelo, J. Gasser, H. Leutwyler, Phys. Rept. **353**, 207 (2001), hep-ph/0005297.
3. G. Colangelo, J. Gasser, H. Leutwyler, Nucl. Phys. B **603**, 125 (2001), hep-ph/0103088.
4. S. Descotes-Genon, N.H. Fuchs, L. Girlanda, J. Stern, Eur. Phys. J. C **24**, 469 (2002), hep-ph/0112088.
5. G. Mahoux, S.M. Roy, G. Wanders, Nucl. Phys. B **70**, 297 (1974).
6. S.M. Roy, G. Wanders, Phys. Lett. B **74**, 347 (1978).
7. N.N. Biswas et al., Phys. Rev. Lett. **18**, 273 (1967).
8. B. Hyams et al., Nucl. Phys. B **64**, 134 (1973) [AIP Conf. Proc. **13**, 206 (1973)].
9. W.J. Robertson, W.D. Walker, J.L. Davis, Phys. Rev. D **7**, 2554 (1973).

<sup>10</sup> See appendix B.2 in [2], equation (B.7).

10. D.H. Cohen, T. Ferbel, P. Slattery, B. Werner, Phys. Rev. D **7**, 661 (1973).
11. M. J. Losty et al., Nucl. Phys. B **69**, 185 (1974).
12. J. Hanlon et al., Phys. Rev. Lett. **37**, 967 (1976).
13. H. Abramowicz et al., Nucl. Phys. B **166**, 62 (1980).
14. G. Veneziano, Nuovo Cim. **57**, 190 (1968);  
C. Lovelace, Phys. Lett. **B28**, 264 (1968);  
J.A. Shapiro, Phys. Rev. **179**, 1345 (1969);  
For a review of this model, we refer to appendix E of [2].
15. M.G. Olsson, Phys. Rev. **162**, 1338 (1967).
16. G. Wanders, Nuovo Cim. **63A**, 108 (1969).
17. E.P. Tryon, Phys. Rev. D **8**, 1586 (1973).
18. J.L. Basdevant, C. Schombly, Phys. Lett. B **45**, 48 (1973).
19. M. R. Pennington and S. D. Protopopescu, Phys. Rev. D **7**, 1429 (1973).
20. J. L. Basdevant, C. D. Froggatt and J. L. Petersen, Nucl. Phys. B **72**, 413 (1974).
21. M.R. Pennington, Annals Phys. **92**, 164 (1975).
22. C. D. Froggatt and J. L. Petersen, Nucl. Phys. B **129**, 89 (1977).
23. W. Ochs,  $\pi$ N Newslett. **3**, 25 (1991);  
AIP Conf. Proc. **1257**, 252 (2010), arXiv:1001.4486.
24. B.S. Zou, D.V. Bugg, Phys. Rev. D **48**, 3948 (1993); *ibid.* D **50**, 591 (1994);  
V.V. Anisovich, D.V. Bugg, A.V. Sarantsev, B.S. Zou, Phys. Rev. D **50**, 1972 (1994); *ibid.* D **50**, 4412 (1994);  
D.V. Bugg, B.S. Zou, A.V. Sarantsev, Nucl. Phys. B **471**, 59 (1996).
25. R. Kamiński, L. Lesniak, K. Rybicki, Z. Phys. C **74**, 79 (1997), hep-ph/9606362.  
R. Kamiński, L. Lesniak, B. Loiseau, Eur. Phys. J. C **9**, 141 (1999), hep-ph/9810386.  
R. Kamiński, L. Lesniak, K. Rybicki, Acta Phys. Polon. B **31**, 895 (2000), hep-ph/9912354.
26. J. Gunter et al. (E852 Collaboration), Phys. Rev. D **64**, 072003 (2001), hep-ex/0001038.
27. N.N. Achasov, G.N. Shestakov, Phys. Rev. D **67**, 114018 (2003), hep-ph/0302220;  
Phys. Rev. Lett. **99**, 07200 (2007), arXiv:0704.2368.
28. F.Q. Wu, B.S. Zou, L. Li, D.V. Bugg, Nucl. Phys. A **735**, 111 (2004), hep-ph/0308152.
29. Z.Y. Zhou, G.Y. Qin, P. Zhang, Z. Xiao, H.Q. Zheng, N. Wu, JHEP **0502**, 043 (2005), hep-ph/0406271.
30. D.V. Bugg, Eur. Phys. J. C **52**, 55 (2007), arXiv:0706.1341.
31. E. Klempt, A. Zaitsev, Phys. Rept. **454**, 1 (2007), arXiv:0708.4016.
32. J.R. Peláez, F.J. Ynduráin, Phys. Rev. D **68**, 074005 (2003), hep-ph/0304067.
33. I. Caprini, G. Colangelo, J. Gasser, H. Leutwyler, Phys. Rev. D **68**, 074006 (2003), hep-ph/0306122.
34. J.R. Peláez, F.J. Ynduráin, Phys. Rev. D **69**, 114001 (2004), hep-ph/0312187; *ibid.* D **71**, 074016 (2005), hep-ph/0411334.
35. R. Kamiński, J. R. Peláez, F. J. Ynduráin, Phys. Rev. D **74**, 014001 (2006) [Erratum-*ibid.* D **74**, 079903 (2006)], hep-ph/0603170.
36. R. Kamiński, J.R. Peláez, F.J. Ynduráin, Phys. Rev. D **77**, 054015 (2008), arXiv:0710.1150.
37. R. García-Martín, R. Kamiński, J.R. Peláez, J. Ruiz de Elvira, F.J. Ynduráin, Phys. Rev. D **83**, 074004 (2011), arXiv:1102.2183.
38. Paper on the  $\pi\pi$  partial waves, in preparation.
39. I. Caprini, G. Colangelo, H. Leutwyler, Int. J. Mod. Phys. A **21**, 954 (2006), hep-ph/0509266.
40. H. Leutwyler,  $\pi\pi$  scattering, in Chiral Dynamics 2006, Proceedings of the 5th International Workshop on Chiral Dynamics, Theory and Experiment, ed. by M.W. Ahmed, H. Gao, H.R. Weller and B. Holstein (World Scientific, 2007), p. 17, hep-ph/0612112.
41. I. Caprini, *Regge analysis of the pion-pion amplitude*, in Chiral Dynamics 2006, Proceedings of the 5th International Workshop on Chiral Dynamics, Theory and Experiment, ed. by M.W. Ahmed, H. Gao, H.R. Weller and B. Holstein (World Scientific, 2007), p. 245.
42. G. Colangelo, PoS **KAON**, 038 (2008), arXiv:0710.3050.
43. G. Colangelo, Nucl. Phys. A **827**, 228C (2009).
44. S.C. Frautschi, *Regge Poles and S-Matrix Theory* (W.A. Benjamin, INC, 1963).
45. R. Serber, Phys. Rev. Lett. **13**, 32 (1964).
46. V. Barger, M. Olsson, D.D. Reeder, Nucl. Phys. **B5**, 411 (1968).
47. W. Rarita et al., Phys. Rev. **165**, 1615 (1968).
48. R.P. Worden, Phys. Lett. **40B**, 260 (1972).
49. V.N. Gribov, Sov. Phys. JETP **26**, 414 (1968) [Zh. Eksp. Teor. Fiz. **53**, 654 (1967)].
50. G.Y. Chou, J. Rix, Phys. Rev. **184**, 1714 (1969).
51. G.L. Kane, A. Seidl, Rev. Mod. Phys. **48**, 309 (1976).
52. A.C. Irving, R.P. Worden, Phys. Rept. **34**, 117 (1977).
53. P.D.B. Collins, *An Introduction to Regge Theory and High Energy Physics* (Cambridge University Press, 1977).
54. A. Donnachie, P. V. Landshoff, Nucl. Phys. B **244**, 322 (1984).
55. A. Donnachie, P.V. Landshoff, Phys. Lett. B **296**, 227 (1992).
56. For a review, we refer to J.R. Forshaw, D.A. Ross, *Quantum Chromodynamics and the Pomeron* (Cambridge University Press, 1997).
57. A. Donnachie, P.V. Landshoff, Phys. Lett. B **437**, 408 (1998).
58. D.E. Groom et al. (Particle Data Group), Eur. Phys. J. C **15**, 1 (2000).
59. P. Desgrolard, M. Giffon, E. Martynov, E. Predazzi, Eur. Phys. J. C **18**, 555 (2001), hep-ph/0006244.
60. O. Nachtmann, Pomeron Physics and QCD, in *Proceedings of Tegernsee 2003, New trends in HERA physics*, p. 253, hep-ph/0312279.
61. S. Donnachie, G. Dosch, P. Landshoff, O. Nachtmann, *Pomeron Physics and QCD*, (Cambridge University Press, 2002).
62. J.R. Cudell et al., Phys. Rev. D **65**, 074024 (2002), hep-ph/0107219
63. Table 41.2 in reference [64].
64. K. Nakamura et al. (Particle Data Group), J. Phys. G **37**, 075021 (2010) and 2011 partial update for the 2012 edition.
65. A. Szczurek, N.N. Nikolaev, J. Speth, Phys. Rev. C **66**, 055206 (2002), hep-ph/0112331.
66. F. Huang, A. Sibirtsev, S. Krewald, C. Hanhart, J. Haidenbauer, U.G. Meissner, Eur. Phys. J. A **40**, 77 (2009), arXiv:0810.2680.
67. C. Bourrely, J. Soffer, T.T. Wu, Eur. Phys. J. C **28**, 97 (2003), hep-ph/0210264.
68. A. A. Godizov and V. A. Petrov, JHEP **0707**, 083 (2007), arXiv:hep-ph/0701121.
69. A. A. Godizov, Phys. Atom. Nucl. **71**, 1792 (2008) [Yad. Fiz. **71**, 1822 (2008)].

70. A. E. Sobol, R. A. Ryutin, V. A. Petrov and M. Murray, *Eur. Phys. J. C* **69**, 641 (2010), arXiv:1005.2984.
71. J.R. Cudell, A. Lengyel, E. Martynov, *Phys. Rev. D* **73**, 034008 (2006), hep-ph/0511073.
72. V.A. Okorokov, *Slope analysis for elastic nucleon-nucleon scattering*, arXiv:0907.0951.
73. M. Ishida, K. Igi, *Phys. Rev. D* **79**, 096003 (2009). arXiv:0903.1889.
74. F. Halzen, K. Igi, M. Ishida, C.S. Kim, *Total hadronic cross sections and  $\pi^+\pi^\pm$  scattering*, arXiv:1110.1479.
75. A. Sibirtsev, J. Haidenbauer, H.W. Hammer, S. Krewald, U.G. Meissner, *Eur. Phys. J. A* **45**, 357 (2010), arXiv:0911.4637.
76. S. W. MacDowell and A. Martin, *Phys. Rev.* **135**, B960 (1964).
77. G. Auberson, A. Martin and G. Mennessier, *Phys. Lett. B* **67**, 75 (1977).
78. S. Weinberg, *Phys. Rev. Lett.* **17**, 616 (1966).
79. J. Gasser, H. Leutwyler, *Phys. Lett. B* **125**, 325 (1983); *Annals Phys.* **158**, 142 (1984).
80. J. Bijnens, G. Colangelo, G. Ecker, J. Gasser, M.E. Sainio, *Phys. Lett. B* **374**, 210 (1996), hep-ph/9511397.
81. J.F. Donoghue, J. Gasser, H. Leutwyler, *Nucl. Phys. B* **343**, 341 (1990).
82. Proc. Int. Workshop on Chiral Dynamics, Bern (2009):  
S. Giudici, *pion pion scattering lengths measurement at NA48-CERN*, PoS(CD09)002;  
V. Yazkov, *Investigation of  $\pi^+\pi^-$  and  $\pi K$  atoms at DIRAC*, PoS(CD09)003;  
B. Bloch-Devaux, *Precise tests of chiral perturbation theory from  $K_{e4}$  decays by the NA48/2 experiment*, PoS(CD09)041.
83. J.R. Batley et al. (NA48/2 Collaboration), *Eur. Phys. J. C* **70**, 635 (2010).
84. S. Pislak et al. (BNL-E865 Collaboration), *Phys. Rev. Lett.* **87**, 221801 (2001) [Erratum-ibid. **105**, 019901 (2010)].
85. J.R. Batley et al. (NA48/2 Collaboration), *Eur. Phys. J. C* **64**, 589 (2009), arXiv:0912.2165.
86. B. Adeva et al., *Phys. Lett. B* **704**, 24 (2011), arXiv:1109.0569.
87. S. Descotes-Genon, N. H. Fuchs, L. Girlanda and J. Stern, *Eur. Phys. J. C* **24**, 469 (2002), arXiv:hep-ph/0112088.
88. S.R. Beane et al. (NPLQCD collaboration), *Phys. Rev. D* **77**, 014505 (2008), arXiv:0706.3026; *The  $I=2$   $\pi\pi$  S-wave scattering phase shift from Lattice QCD*, arXiv:1107.5023.
89. X. Feng, K. Jansen, D.B. Renner, *Phys. Lett. B* **684**, 268 (2010), arXiv:0909.3255.
90. T. Yagi, S. Hashimoto, O. Morimatsu, M. Ohtani,  *$I=2$   $\pi\pi$  scattering length with dynamical overlap fermion*, arXiv:1108.2970.
91. G. Colangelo et al. (FLAG Working Group), *Eur. Phys. J. C* **71**, 1695 (2011), arXiv:1011.4408.
92. G. Antchev et al. (TOTEM Collaboration), *Europhys. Lett.* **95**, 41001 (2011), arXiv:1110.1385.
93. M. M. Block and F. Halzen, *Phys. Rev. D* **83**, 077901 (2011), arXiv:1102.3163.
94. M. M. Block and F. Halzen, *Experimental confirmation that the proton is asymptotically a black disk*, arXiv:1109.2041.
95. N.N. Achasov and A.V. Kiselev, *Phys. Rev. D* **83**, 054008 (2011), arXiv:1011.4446;  
*Analytical properties of the  $\pi\pi$  scattering amplitude and the light scalar mesons*, talk given at QUARKS 2010, Kolomna, Russia, arXiv:1009.5551.
96. A. V. Anisovich et al., *Sigma-meson and confinement singularity*, arXiv:1105.5923.
97. I. Caprini, *Phys. Rev. D* **77**, 114019 (2008), arXiv:0804.3504.
98. R. Garcia-Martin, R. Kaminski, J. R. Pelaez and J. Ruiz de Elvira, *Phys. Rev. Lett.* **107**, 072001 (2011), arXiv:1107.1635.
99. B. Moussallam, *Couplings of light  $I = 0$  scalar mesons to simple operators in the complex plane*, arXiv:1110.6074;  
*Properties of light scalar mesons in the complex plane*, talk given at Hadron 2011, Munich, Germany, arXiv:1108.4640.
100. H. Leutwyler, *AIP Conf. Proc.* **1030**, 46 (2008), arXiv:0804.3182.
101. W. Flatté, *Phys. Lett.* **63B** 224 (1976).